Optimization of zirconia-based pastes for additive manufacturing of dental prosthesis

Madalena Afonso Vilar de Castro Paredes

Thesis to obtain the Master of Science Degree in

Bioengineering and Nanosystems

Supervisor: Doctor Ana Paula Valagão Amadeu do Serro

Supervisor: Doctor Célio Gabriel Figueiredo-Pina

Examination Committee

Chairperson: Doctor Gabriel António Amaro Monteiro
Supervisor: Doctor Célio Gabriel Figueiredo-Pina
Members of the Committee: Doctor Ana Mafalda Saldanha Guedes

December 2017

Acknowlegments

This master thesis was only possible due to some people's contribution, who directly or indirectly helped me on this project. I would like to express my gratitude for their support throughout this journey.

First of all, I am deeply grateful to my supervisors Doctor Ana Paula Serro and Doctor Célio Figueiredo-Pina, who had always showed an extraordinary availability and patience. I would like to thank both for the encouragement and for being tireless along these months. Also, I would like to thank for giving me this opportunity, which has contributed for my professional growth.

To Doctor José Mata, I would like to thank for his availability and help when it was needed.

I would like to thank to Professor Anabela Raymundo for all the availability with the rheometer and for helping me whenever I needed to. To my college Rita Faustino and her supervisors, for giving me access to CTN and for all the assistance. To Doctor Rogério Colaço and Doctor Mário Polido for the availability on some devices.

For all the support and wisdom, I would like to thank to Engineer Marco Medeiros.

My gratitude goes also to all my laboratory colleagues, Diana Silva, Ana Topete, Diogo Silva, Mariana Freire and Sofia Oliveira for all the help, integration and good disposition.

A special thanks goes to Ana Catarina Branco, for her friendship, encouragement and motivation. Thank you for helping me whenever I needed to. Without you, this journey would not have been the same.

Finally, a huge thanks to my generous family, especially to my parents and my sister who made all my accomplishments possible, for their exceptional support and unconditional love. Everything I've achieved I owe it to you.

Abstract

Dental restorations are often used to solve function and aesthetic problems of native teeth. As restorative materials, ceramics became increasingly popular because of their aesthetics, inertness, mechanical properties and biocompatibility. Additive manufacturing, namely robocasting, of ceramic materials has gained significant interest to produce customized pieces, leading to low time of processing and materials consumption.

The main objective of this work was the optimization of zirconia-based pastes to produce dental prosthesis through the robocasting 3D technology. The rheology of several pastes (zirconia-based pastes, containing the dispersant Dolapix CE64 and an additivative zirconia-based paste supplied by CTCV) was studied, concerning the amount of dispersant, the method of preparation and the solids content. Density and porosity measurements, as well as preliminar printability tests, were carried out. In addition, topography/morphology, wettability, tribological behavior, microhardness and toughness were also evaluated and compared with commercial zirconia.

Overall, taking into account the preliminary test of printability, the results showed that specimens produced with paste containing 92% solids and 1% Dolapix may be used for production of dental parts by robocasting, since the produced specimens present adequate properties for dental applications, with roughness values of 6.53 nm, microhardness values above 1100HV and toughness values between 3–6.5 $Pa \cdot m^{1/2}$.

Key words: Additive manufacturing, robocasting, dental restorations, zirconia pastes, materials characterization.

Resumo

As restaurações dentárias são frequentemente usadas para resolver problemas funcionais e estéticos de dentes nativos. Como materiais restauradores, a cerâmica tornou-se cada vez mais popular devido à sua estética, inércia, propriedades mecânicas e biocompatibilidade. O fabrico de aditivos de materiais cerâmicos, nomeadamente por *robocasting*, ganhou interesse significativo para produzir peças personalizadas, resultando num reduzido tempo de processamento e consumo de materiais.

O principal objetivo deste trabalho foi a otimização de pastas à base de zircónia para produzir próteses dentárias através da tecnologia de impressão 3D por *robocasting*. Estudou-se a reologia de várias pastas (pastas à base de zircónia, contendo o dispersante Dolapix CE64 e uma pasta aditivada à base de zircónia fornecida pelo CTCV), quanto à quantidade de dispersante, ao método de preparação e ao conteúdo de sólidos. Foram realizadas medidas de densidade e porosidade, bem como testes preliminares de printabilidade. Além disso, a topografia/morfologia, molhabilidade, comportamento tribológico, microdureza e tenacidade também foram avaliadas e comparadas com zircónia comercial.

No geral, tendo em consideração o teste preliminar de imprimibilidade, os resultados mostraram que os espécimes produzidos com pasta contendo 92% de sólidos e 1% de Dolapix podem ser usados para a produção de peças dentárias por *robocasting*, uma vez que os mesmos apresentam propriedades adequadas para aplicações dentárias, com valores de rugosidade de 6.53 nm, valores de microdureza acima de 1100HV e valores de tenacidade entre 3–6.5 $Pa \cdot m^{1/2}$.

Palavras-chave: Manufactura aditiva, *robocasting*, restaurações dentárias, pastas de zircónia, caracterização de materiais.

Table of Contents

List of Figures

List of Tables

List of Abbreviations

AM – Additive Manufacturing

2D – Two Dimensional

3D – Three Dimensional

DEJ – Dentine-ename junction

Y-TZP – Yttrium cation-doped Tetragonal polycrystalline zirconia

CAD/CAM – Computer Aided Design/ Computer Aided Manufacturing

ZTA – Zirconia-Toughened Alumina

Mg-PSZ – Magnesium cation-doped partially stabilized zirconia

SM – Substrative Manufacturing

CNC – Computer numerically controlled

LDM – Liquid Deposition Modeling

DIW – Direct Ink Writing

RP – Rapid Prototyping

CT – Computer tomography

STL – Stereolithography

CTCV – Centro Tecnológico de Cerâmico e do Vidro

AFM – Atomic Force Microscope

SEM – Scanning Electron Microscope

Chapter 1 – Theoretical Introduction

Human teeth are not only an important masticatory organ, but are also closely associated with the pronunciation and facial aesthetics of humans. Thus, teeth play an extremely vital role in our daily life. With ageing, various pathological factors and traumas, dental lesions such as caries, partial or total loss of tooth tissue will inevitably occur. As a result, artificial dental materials, *e.g.* crowns, have been gradually developed and used to restore and treat lesions of human teeth. [1]

The recent introduction of additive manufacturing (AM) techniques in the dental field has marked a turning point in the prosthesis production technology, from the traditional hand made to the innovative automated approach. [2] This 3D technology has the advantage of being faster and more efficient and leads to less waste material. The speed and ease of use of this process opens the possibility to be the own dentist to fabricate custom dental crowns in his office. However, the use of this technique for producing crowns is still quite incipient. One of the main reasons has to do with the need of materials optimization, which should present appropriate characteristics to be processed through the 3D technology and simultaneously mimic the natural tooth. Currently, metals and alloys, ceramics and composite materials are the most widely used for dental restorations and implants [1], but only polymers are being used in AM.

In order to develop new dental restorative materials, it is imperative to evaluate and understand the structure-property relationships of the human tooth. [3] In fact, to restore the mechanical function of tooth it is not only important to study its intrinsic properties, including the bulk structural behavior, but also to understand the mechanisms by which tooth structures resist functional forces in the mouth. Thus, both mechanical properties and microstructural features of teeth are important to perceive stress dissipation in the tooth, for developing biomimetic restorative materials and for the execution of clinical dental pieces.

The main objective of this work is the optimization of zirconia-based pastes to produce dental prosthesis through 3D technology. The main challenge of the work will be the development of printable materials, with adequate mechanical and structural properties that meet the demanding requirements for dental crowns restoration. Suspensions of zirconia particles will be used to create pastes. Different production parameters will be tested, as the suspension solid content, the amount of dispersive agent, or the effect of the presence of other aditives. Several characterization techniques will be applied to study the properties of the obtain materials and infer about the possibility of producing dental crowns with the materials under study, namely measurements of porosity, hardness, wettability, tribological behaviour and surface morphology.

1.1 Human teeth

Human teeth have the main functions of cutting, tearing and grinding food, functioning in this way as a mechanical device during the chewing process. [3] They present two distinct parts, the crown and the root, being attached in a strangulated intermediate portion called the colon. Figure 1 shows a schematic diagram of a healthy tooth. These parts are composed by two anisotropic structures: a calcified one, (comprising enamel and dentin) and a non calcified (the pulp). Thus, the two most important elements of a tooth that determine its resistance to the severe conditions found in the mouth are the external enamel and the subjacent dentine. [1]

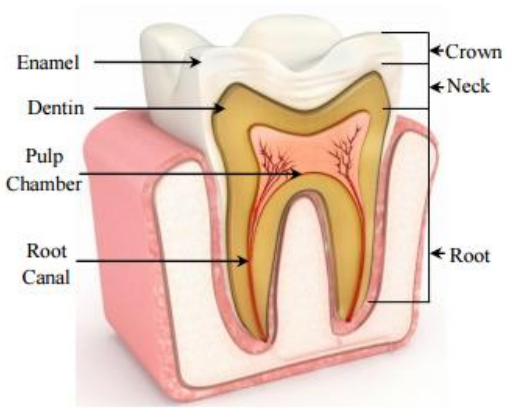

Figure 1. Schematic sectional view of an human healthy tooth. [4]

1.1.1 Tooth microstructure

From advanced materials science perspective, a tooth is a functionally graded composite material with mineralized matrix and organic reinforcement. [3], [4] Dentin and enamel are calcified layered structures which are bonded by a functional graded dentine-enamel junction (DEJ) layer. [4]

The crowns of human teeth are covered by dental enamel [3], which is the hardest tissue in the human body. Dentine is normally considered to be more elastic and soft. [1]

Enamel contains on average 95% inorganic substance, 4% water and 1% organic substances by weight. Hydroxyapatite which is a crystalline calcium phosphate, is the main mineral constituent. Its stoichiometric form is $[Ca_{10}(PO_4)_6OH_2]$. However, it is known that in the enamel the hydroxyapatite is non-stoichiometric, being $[(Ca, M)_{10}(PO_4, Y)_6(OH, X)_2]$; where M = Mg^{2+}, Na^{+}, K^{+}, Sr^{2+}, Ba^{2+}; Y = CO_3^{2-}, $H_2PO_4^{-}$, HPO_4^{2-}, SO_4^{2-} and X = F^{-}, Cl^{-} and CO_3^{2-}. [5] Both enamel protein and water are more abundant in inner enamel close to the dentine-enamel junction. Human teeth enamel consists of aproximately 5 µm diameter rods encapsulated by aproximately 1 µm thick protein rich sheaths that are arranged parallel in a direction perpendicular to the dentin-enamel junction from dentin to the outer

enamel surface. In the central part of the rod, crystallite plates are parallel to the rod axis while those near the edge of the rod usually have an angle near 15-45° to the longitudinal axis of the rods. The rod unit is the most important part for the understanding the microstructure and function of enamel. [6], [7]

Dentine, a hydrated biological composite mostly made of phosphoric apatite crystallites, is the main supporting structure of the tooth and is the second hardest tissue in the body after enamel. In its composition, it has about 70% inorganic material, 18% organic material and 12% water. [6] It is considered an elastic and soft part of the tooth that contains dentinal tubules, which extend through its entire thickness. The tubules are surrounded by highly mineralized cylinders of peritubular dentine in the crown, which are, in turn, separated by intertubular dentin. [3]

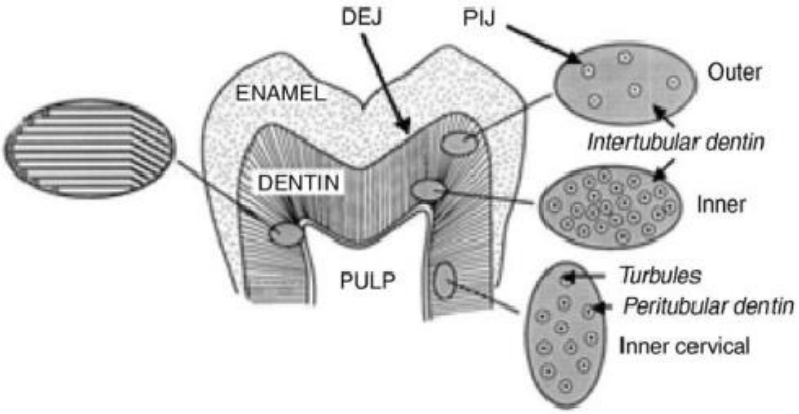

Figure 2. Schematic diagram of the tooth with important interfaces. [8]

The dentin-enamel junction (DEJ), which is normally considered as the biological interfacial region between the dentin and outer enamel coating in teeth [9], is a unique junction between highly mineralized tissues of different physical properties, embryogenic origins and matrix composition. [4]

1.1.2 Mechanical and tribological behaviour of natural tooth

Knowledge of the mechanical properties of human teeth is of utmost importance when considering clinical treatment. It also guides the development of "tooth-like" restorers that mimic the structure and properties of teeth. [10]

It has been experimentally verified that both enamel and dentin have a fragile behavior. The mode of enamel fracture is highly anisotropic but, fot dentin it is less anisotropic. [10] In other words, the anisotropic microstructure of the enamel, resultant from rod orientation and the presence of organic components, controls the ability of its antifracture. An extensive bibliographic research reveals that advanced characterization techniques were used to record the mechanical response of the different anatomical parts of the human tooth. However, there is still a lack of correlation between basic

mechanical properties, such as hardness, and microstructural composition of various structural parts of the human tooth. [3], [10] The main mechanical mechanical properties of enamel and dentine are referred in Table 1. As already mentioned, enamel is the hardest tissue in the human body with a Knoop hardess of about 250 – 500, equivalent to 5 times that of dentin (57–71 KHN). [11] Enamel is brittle and easily broken if it loses the support of the flexible dentin below, so the combination of enamel and dentin is very important to be able to withstand about a 20 MPa occlusion pressure approximately 3000 times per day. Therefore, enamel must retain its shape as well as its fracture resistance and wear during load-bearing function for the life of the individual. Understanding enamel fracture properties and its crack propagation is crucial for both clinicians and materials scientists and helps in the clinical management of tooth wear, which involves replacing missing dental tissue with dental materials, along with an attempt to minimize causal factors. [6]

Table 1. Mechanical properties of enamel and dentine. [1], [7], [12]

Property	Enamel	Dentine
Young's modulus (GPa)	20.0 – 84.2	10.2 – 15.6
Shear modulus (GPa)	29	6.4 – 9.7
Tensile Strength (GPa)	0.030 – 0.035	0.040 – 0.276
Compressive Strength (GPa)	0.095 – 0.386	0.249 – 0.315
Shear Strength (GPa)	0.06	0.012 – 0.138
Knoop hardness	250 – 500	57 – 71
Density (Kg/m^{-3})	2500	2900

Another important property to be critically considered is the tribological behaviour, once oral biomechanical functions can usually result in some relative movement between contacting surfaces that can be teeth, restorations and implants. [3] Tribology is the science of the mechanisms of friction, lubrication and wear of interacting surfaces that are in relative motion. [1] Basically, the tribological response, being a system dependent property for a given tribocouple, depends on the mechanical properties of both coupling solids (*e.g.*, E-modulus, hardness and toughness). The transmission of forces, energy conversion and alteration of the mechanical and chemical properties results in an eventual removal of material. Thus, understanding of wettability, friction and wear behavior of human teeth helps in the development of new dental restorative materials. [3]

1.1.2.1 Friction and Wear

Regarding teeth, due to their location and biomechanical function in the chewing processes, tribological movements can occur which cause friction and wear of the teeth. [1], [12] Friction is, by definition, the sliding of one object or surface against another, whereas wear is a process that occurs whenever a

surface is exposed to another surface or chemically active substances [13], which can result in a progressive removal of the surface material by mechanical or chemical action. [1] Tooth wear is a multifactorial phenomenon involving the interplay of biological, mechanical and chemical factors. [1], [14] which means that the etiology of tooth wear and restorations vary depending upon joint pathology, occlusion, muscle tune, lubricants, individual dietary habits, and the type of restorative material used. [15], [16] In this way, friction and wear may result from direct contact between the teeth and particles during mastication or from pathological processes such as bruxism (which is is the action of grinding of teeth without the presence of food), toothbrushing and others, whose scheme is represented in Figure 3.

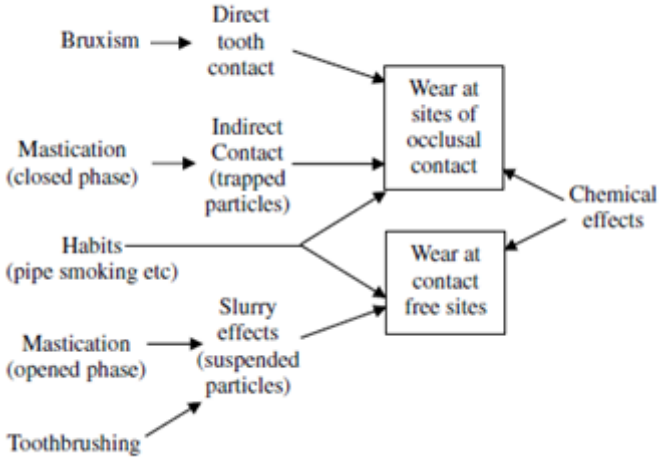

Figure 3. Summary of clinical wear mechanisms. Adapted from [16]

1.1.2.2 Wettability/Oral Environment

The oral environment has great importance in dental tribology [1] because saliva provides protection against physical and chemical wear. Saliva acts as a lubricant that provides a reduction in friction between teeth and food, between teeth themselves and between teeth and the oral mucosa/tongue and preserving, at the same time, deglutition, chewing and the faculty of speech. [12], [17] In turn, wettability, which is a surface characteristic known to affect the biological response of teeth or dental prostheses, is closely related to the oral environment. [18] In general, wettability is quantified by the contact angle, which is the angle between the tangent line to a liquid drop's surface at the threephase boundary and the horizontal solid's surface, which defines whether the material is hydrophilic or hydrophobic. The contact angle for water on a solid surface is regarded as a natural phenomenon and mainly depends on the chemical composition and the structure of materials. Although there is lack of relevant research about enamel substrates, some studies have been reported [12], [19], [20], where the enamel surface is considered hydrophilic.

In this way, due to the need for greater durability of teeth and dental restorative materials, its important to take into consideration the surface wettability to control properties like adhesion, lubrication, friction, wear resistance and biocompatibility. However, the wettability of surfaces can be strongly affected by surface roughness in many different ways, so this influence can be very significant and must be taken under consideration. [21] Considering that the roughness is related to the surface preparation, porosity must be also taken into account. These surface characteristics are of clinical importance since a manipulation of these variables might facilitate the prevention of dental disease by avoiding dental plaque formation, which is a microbial plaque.

1.2 Artifical dental materials

Due to various pathological factors and traumas, patients may suffer dental injuries. To address this problem, various artificial materials have been developed to be used in dentistry, in order to replace missing teeth or non-esthetic but healthy tooth tissue and tooth enamel. Some examples are shown in Figure 4. The practical goals of these treatments are based on the recreation not only of the function but also of the aesthetics. To select a material for dental application, it is necessary to take into consideration that the choice depends on several factors, such as corrosion behavior, mechanical properties, including strength and wear, cost, availability, biocompatibility and aesthetic values. Usually dental materials can be grouped into four categories: metals and their alloys, ceramics, polymers and composites. [1] Despite the good long-term results, the moderate aesthetics and biocompatibility concerns associated with the metals have increased the use of other materials. [22] Dental literature indicates that ceramics are considered one of the most suitable materials to be used in dental restorations. [23]

Figure 4. Types of dental crowns. [24]

1.2.1 Ceramic materials in prosthodontics

Within the dental field, ceramics offers advantages regarding their own nature and their chemical and optical properties. Ceramic materials are highly resistant to acid and corrosion attacks and are therefore regarded as exceptionally biocompatible. Furthermore, ceramics have a high resistance against wear and, recently, due to the increasing aesthetic demand, the use of all-ceramic prostheses (like full-coverage crown) has become popular [23]. Aesthetics is an obvious attribute of some ceramics and, along with biocompatibility, durability and etchability (ability to be bonded), are the primary reasons why dentists often choose ceramics over other materials. [1], [23].

However, there are relevant issues that arise in the dental use of such material. These problems are related to its potential for catastrophic brittle fracture as well as its potential for abrasion of opposing natural teeth or restorations, leading to a poor durability. In order to minimize damage from brittle fracture, many efforts have been made in the last decades to develop high strength dental ceramics. Feldsphatic porcelain, leucite reinforced felspathic porcelain, magnesia based porcelain, lithium disilicate glass-ceramic, polycrystalline ceramics (as alumina and zirconia, which does not have glassy matrix), and others, are some examples of these developed ceramics. [25] In addition, tetragonal polycrystalline zirconia (Y-TZP), a high hardness zirconia ceramic, was developed as an alternative to porcelain or glass ceramics in posterior restorations, raising particular interest [1] due to its great resistance to fracture when compared to other materials. Figure 5 and Table 2 report several studies made for fracture force, flexural strength and frature thoughness for some of these materials. In addiction, zirconia's biocompatibility has been proved both *in vitro* and *in vivo* as a non-cytotoxic and non-mutagenic material, and no local or systemic adverse reactions have been identified. [22]

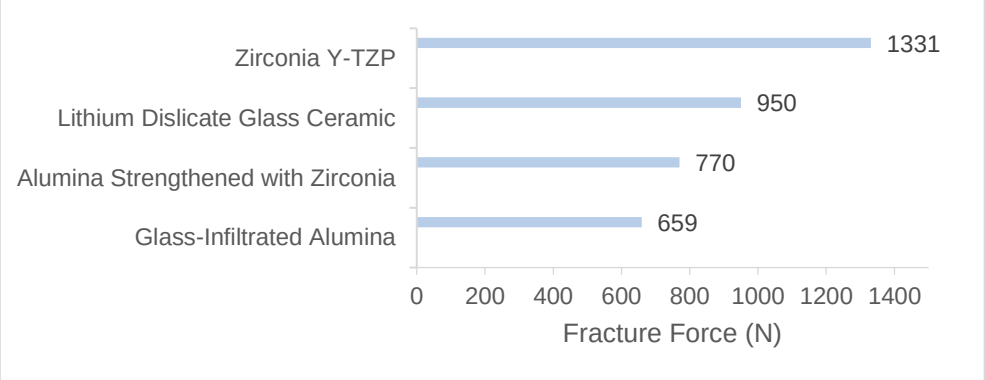

Figure 5. Literature values for fracture force (not under exact same conditions). Adapted from [26]

Table 2. Mechanical properties of the most used ceramic materials in fixed prosthodontics. Adapted from [22]

Ceramic system	**Reinforcing material**	**Flexural strength (MPa)**	**Fracture toughness (MPa/m$^{1/2}$)**
Glass-ceramics	Feldsphatic porcelain	100	1.0
Glass-ceramics with fillers	Leucite	160	1.5 – 1.7
	Lithium disilicate	300 – 400	2.8 – 3.5
Crystalline ceramics with glass fillers	Glass-infiltrated alumina	236 – 600	3.1 – 4.6
	Glass-infiltrated zirconia toughened alumina	421 – 800	6 – 8
Polycrystalline ceramics	Densely sintered alumina	487 – 699	4.48 – 5.6
	Yttria stabilized zirconia	900 – 1200	9 – 10

1.2.1.1 Zirconia-based ceramic

Zirconia, due to its excellent mechanical properties, holds a unique place amongst ceramic oxides. This situation stems from the considerable amount of research work that has been conducted since the discovery of the transformation toughening capabilities of zirconia in the mid-1970s. [27]

Under ambient pressure, the temperature influences the crystallographic form of unalloyed zirconia, allowing it to assume three crystallographic forms: pure zirconia phase or monoclinic phase ***(m)*** (a deformed prism with parallelepiped sides); tetragonal phase ***(t)*** (a straight prism with rectangular sides) and cubic phase ***(c)*** (square sides). At room temperature and upon heating up to 1170 °C, the structure is monoclinic. Then it is tetragonal between 1170 and 2370 °C and cubic above 2370 °C and up to the melting point. [27] The best mechanical properties of zirconia are achieved only if some grains are able to transform under stress from the tetragonal metastable state towards the stable monoclinic state, concept which is called phase transformation toughening. In other words, zirconia can be used as a structural bioceramic only if it is not completely stable. However, upon cooling, transformation from the tetragonal (*t*) phase to the monoclinic (*m*) phase will induce a substantial increase in volume (~4.5%), which will lead to catastrophic failure. Even so, this necessary metastability in a moist environment, may cause a spontaneous transformation from the metastable tetragonal phase to the stable monoclinic phase, decreasing the strength of the material, phenomenon which is called aging (or low temperature degradation) as shown in Figure 3. [22],[27] Researchers found that the addiction of CaO, MgO, Y_2O_3 or CeO_2 to zirconia-alloys allows the retention of the tetragonal structure at room temperature. This will control the stress-inducing ***t→m*** transformation, which induces compressive stresses, thereby closing the crack tip, preventing further crack propagation and leading to high toughness. [28]–[30] Also, the addiction of stabilizers can prevent or decrease aging. [22] This unique characteristic gives zirconia superior mechanical properties compared to other dental ceramics.

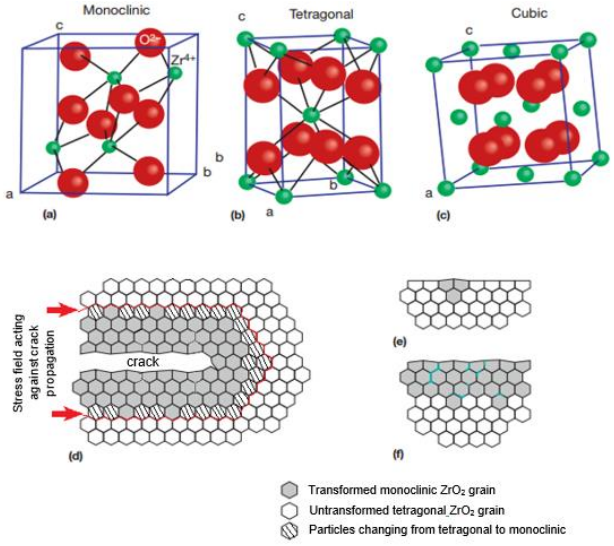

Figure 6. (a–c) The three major polymorphs of zirconia, and the two alternative means by which metastable tetragonal phase can transform to monoclinic phase. (d) Phase transformation toughening and (e, f) aging. Adapted from [27]

Thus, new materials and technologies to process zirconia based ceramics, such as CAD/CAM, have been developed. [23] In vitro studies demonstrated a flexural strength of 900–1200MPa and a fracture toughness of 9–10MPa.$m^{1/2}$. [30] However, these parameters may change depending on the treatment of the restorative material (exemplified in Figure 7), as shown for flexural strength in Table 3. [29]

Table 3. Restorative zirconia based materials used for CAD/CAM systems. [29]

Restorative material	Flexural strength (MPa)
In-Ceram Zirconia (zirconium oxide)	750
Partially sintered zirconia (zirconium oxide)	800 – 1300
Full sintered zirconia (zirconium oxide)	>1000

The recent introduction of ceramic-based zirconia as dental restorative materials has generated considerable interest in the dental community. [28] Although there are several types of zirconia-containing ceramic systems currently available, to date only three are used in dentistry. These are yttrium cation-doped tetragonal zirconia polycrystals (3Y-TZP), zirconia-toughened alumina (ZTA) and magnesium cation-doped partially stabilized zirconia (Mg-PSZ), whose properties are presented in Table 4. [28]

Table 4. Mechanical properties of 3 types of zirconia used in dentistry. [12]

Property	Y-TZP	ZTA	Mg-PSZ
Young Modulus (GPa)	210	380	210
Compressive Strength (GPa)	2		2
Density (Kg/m^{-3})	6000	4150	5850
Flexural strength (MPa)	950		600
Flexural strength (MPam$^{1/2}$)	10.5	4–5	5.8
Vickers Hardness ($HV_{0,5}$)	1250	1600 (HV_{30})	1250

By comparing the various parameters of the Table 4 and through some literatures [22],[26], it is possible to conclude that, in general, stabilizing zirconia with yttrium oxide enhances its mechanical properties more than with other oxides. Zirconia can be stabilized partially by 2 – 5 mol% of yttrium oxide or fully by 8 mol% of yttrium oxide. Although, dental zirconia, is commonly partially stabilized. [22]

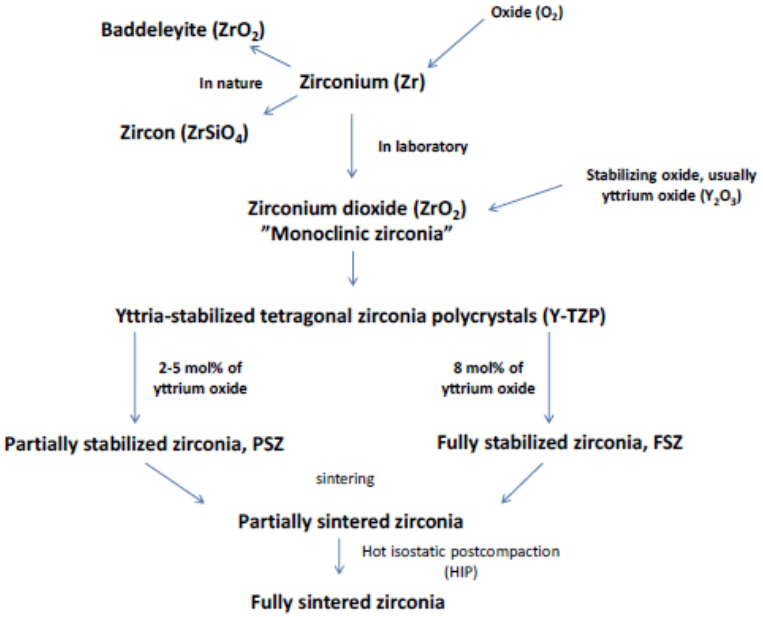

Figure 7. The various states of zirconia. [22]

1.2.1.1.1 Problems related to zirconia restorations

A few clinical problems related to zirconia restorations are known as secondary caries, marginal discoloration, ceramic fractures, chipping of the veneering porcelain and loss of retention. [22] These problems occur in various combinations to cause surface loss of materials in the mouth. Thus, problems associated with restorations are based on crown microstructures, surface characteristics and environmental influences.

Wear and Friction Coefficient

Wear properties of restorative dental materials differ from those of natural teeth and may alter the wear rate of natural opposing teeth. So ideally, the wear resistance of the restorative material and the enamel should be similar. [15] Although zirconia has a high resistance against wear, a possible abrasiveness of this material restorations to antagonist teeth due to its hardness has raised concerns in dentistry. [22] The applied load also has a significant effect on the friction coefficient and wear (*i.e.*, if the surface of the ceramic is already degraded, when subjected to occlusion, the dental wear process will be accelerated).

Oral environment

Given the complex inter-oral environment and biomechanics, the degradation of the zirconia surface can be due to the influence of pH from diet and intrinsic diseases. However, the natural conditions found in the oral cavity (pH and temperature changes) are not severe enough to dissolve components from

this dental ceramic. [31] Low bacterial adhesion of the restoration is a crucial factor in the longevity of the restoration. Crucial factors affecting dental plaque (which is biofilm or mass of bacteria that grows on surfaces within the mouth) adhesion to the dental restoration are the surface roughness of the material and, intimately related to it, the wettability. Less bacterial adhesion has been found on smooth surfaces than on rough ones, and bacterial adhesion to ceramic materials like zirconia has been noted to be low due to their surface characteristics. [22]

1.3 Dental materials processing for restoration

In dentistry, a constant search for new materials and new technologies that improve performance and cost of dental restorations is carried out. [32] Nowadays, there are equipments, like intra-oral and extra-oral scanners, that allow to reproduce the teeth/oral cavity dimensions, being possible to make dental crown molds. However, the quality of intra-oral scanner is not yet satisfactory, because the digitizing process is greatly affected by the clinical and physiological conditions, *e.g.* saliva, blood or patient movements. In addition, the digitization of an oral impression is difficult due to its concave geometries and it can lead to poor virtual representation. The indirect procedure, involving impression taking and replica production, is more precise and therefore stone replica (*i.e.*, plaster mold) is commonly digitized. [2]

Therefore, restorations can be designed from a virtual model of the prepared tooth, using a specific CAD tool. The availability of a geometric model for the restoration allows the production of a dental device through subtractive or additive approaches as Computer Aided Manufacturing (CAM) or Additive Manufacturing (AM) processes. This implies a demand for adaptations or development of materials that follow the needs of the specific technology and the specific indication. [33]

1.3.1 Subtractive Manufacturing

The technology known as Subtrative Manufacturing (SM), is a computer numerically controlled machining, which is based on processes in which power-driven machine tools, such as lathes, saws, milling machines, and drill presses, are used with a sharp cutting tool to mechanically cut the material (removing undesired materials) to achieve the desired forms. [33] Thus, subtractive manufacturing is a process by which 3D objects are constructed by successively cutting material away from a solid block of material (by conventional or unconventional machining), which forces designers to have in mind the limitations of all manufacturing techniques involved on the product. Although it is a technology based on CAD/CAM widely used, this method leads to a great waste because more material is removed compared to what is used in the final product. It also involves tools wear, that require periodic substitution. In this way, on a large scale, this results in relevant environmental problems. [34]

1.3.2 Additive Manufacturing

Additive manufacturing (AM) technology has been studied and developed for more than 20 years. Instead of removing materials, AM processes are responsible for producing three-dimensional parts directly from CAD models by adding materials layer by layer, which allows the building of parts with geometric and material complexities that could not be reproduced by subtractive manufacturing processes. [35] The integration of AM in traditional dental restorations manufacturing is an emerging application. [2] In Figure 8 a flowchart illustrating the different routes in order to produce personalized implants from polymers, metals or ceramics is shown.

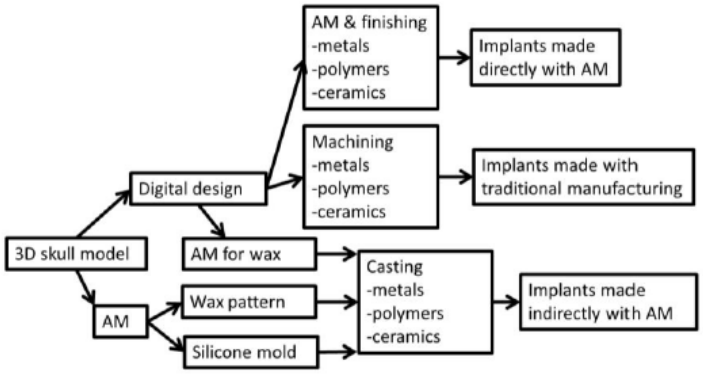

Figure 8. Example of different routes to produce customized implants. [36]

Among the advantages of the additive process over conventional subtractive manufacturing methods is the reduction of the raw material consumption. In fact, while in the subtractive manufacture a block of material is processed by material removal machines, which the result will consequently lead to a large amount of waste material, the volume of raw material used during the AM process is in practice close to the volume of the part before the finishing phase. [33], [34] Other advantages are related with the lower processing time, lower number of production steps and the adequacy to produce complex and personalized pieces. Subtractive vs. additive manufacturing is shown in Figure 9.

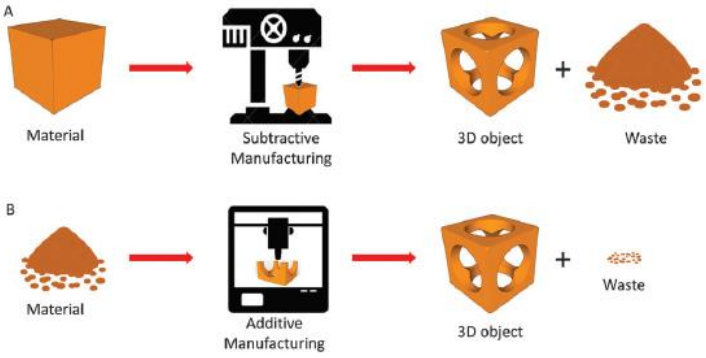

Figure 9. Subtractive manufacturing (A) versus additive manufacturing (B). [36]

A significant advance has been observed in the development and commercialization of new and innovative AM processes, also known as 3-D printing. [35], [37] As shown in Figure 10, the 3D printing process starts when the object's digital model is obtained through CAD software, a 3D scanner or a photogrammetry procedure. The design of the 3D model is then converted to a stereolithography file (STL) format so a cutting process is applied using the printer software to convert the STL file data into a G code file containing geometric information from a series of 2D layers in which the model is divided. Finally, the printer begins to deposit the material following the layer-by-layer sequence dictated by the G code file. [37] This technique has the main advantage of producing details such as undercuts, voids, and complex internal geometries.

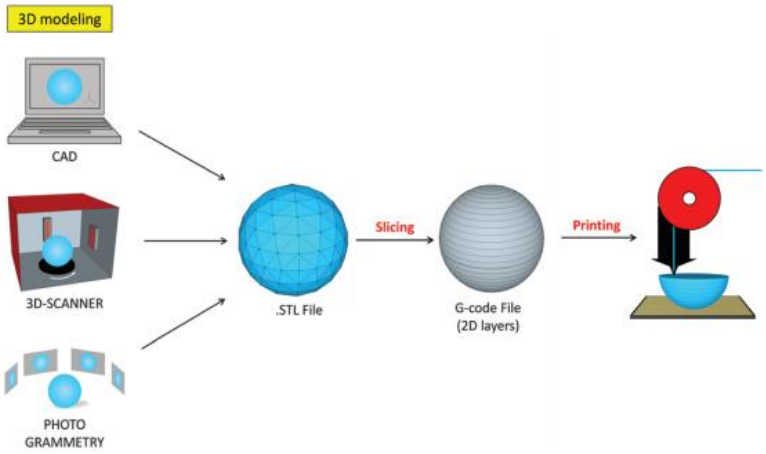

Figure 10. 3-D Printing process. [37]

Addictive manufacturing includes different processing categories. In each one, some technologies can be highlighted, whose characterization is made by specific processing and applications. Some of these 3-D printing methods are listed in Table 5.

Photopolymerization refers to the layer by layer or an entire layer at a time solidification of a curable fluid medium and provides exceptional dimensional tolerance, but cannot manufacture with multiple materials. [38], [39]

In turn, powder bed process is an additive manufacturing technology often also referred to as layer melting. Within this technology can be found several techniques, being one of the most important and used selective laser sintering, where a laser sintering applies a laser energy source to sinter successive powder layers. Although this method results in high quality components with negligible porosity, it is not compatible with multiple materials. [38], [39]

On the other hand, lamination is the process of mechanical conformation that aims to change shape (*i.e.*, thickness), by mass deformation. In this case, the created objects are not so precise and does not have such complex geometries compared to other techniques, which leads to the disadvantage of low quality surface since the individual layers are cut by laser beams. [38]

Finally, the extrusion process generates a three-dimensional object by the deposition of a filament (solidified if it is in FDM, or not solidified if it is DIW) from the movable deposition head, allowing low cost manufacture within a reasonably short build time, and accommodating multiple materials like metals, polymers, and ceramics, being a technique of great success and with a wide application. In addition to the techniques presented, there is also the 3D-printing process of injecting material, which offers high resolution and low polymerization shrinkage and also allows fabrication of objects with a smooth surface. [40]

The choice of the appropriate method to use depends on the consideration of some factors, such as the complexity of the objects to be created, the material used, the number of replicas required and, of course, the cost. [37] The feasibility of these different AM processes, has recently have been investigated for the production of ceramic pieces. [41]

Table 5. Summary of 3-D printing methods for different types of materials. [37]

3D-printing process	Technique	Materials	Advantages	Limitations
Photopolymerization	Stereolithography (SLA)	Photopolymers	Simple	Single material
	Material jetting	Photopolymers	Multimaterial structures	High cost
	Continuous liquid interface printing (CLIP)	UV-curable resins	High speed	Single material
	Two-photon polymerization (2PP)	UV-curable resins	Sub-100 nm resolution	Low yield of production
Extrusion	Fused deposition modeling (FDM)	Thermoplastics (ABS, PLA, PC, PA, *etc.*); glass (new); metal (new)	Simple, multimaterial structures; low cost (for thermoplastic materials)	High cost (for glass and metal)
	Robocasting (DIW)	Plastics, ceramic, food, living cells, composites	Versatile	Requires post-processing; low resolution
Powder based	Selective laser sintering (SLS)	Thermoplastics, metals	No need for support material	Limited mechanical properties of object; high cost
	Selective laser melting (SLM)	Metals	No need for support material	High cost
	Electron beam melting (EBM)	Metals	No need for support material	High cost
	Binder jetting	Any material in particulate form	No need for support material; versatile; lower cost than laser-based methods	Limited mechanical properties
	Selective inhibition sintering (SIS)/inhibitor jetting	Metal	Sintering is performed only once after printing; lower cost than laser-based methods	Low resolution; limited mechanical properties
Lamination	Laminated object manufacturing (LOM)	Paper, metal, plastic, *etc.* as laminated sheets	Versatile	Limited mechanical properties; some design limitations

Therefore, the current dental CAD/CAM systems is not the best choice for mass production of crowns and bridges since only one part can undergo machining at once. [32] In this perspective, Additive Manufacturing is a great opportunity for the dental industry in the production of custom parts specially made for the patient, where robocasting of ceramic materials has room for improvement. Although some challenges are not explored yet, there is already several of additive manufacturing technologies that can be used in dentistry (some examples are shown in the Figure 11).

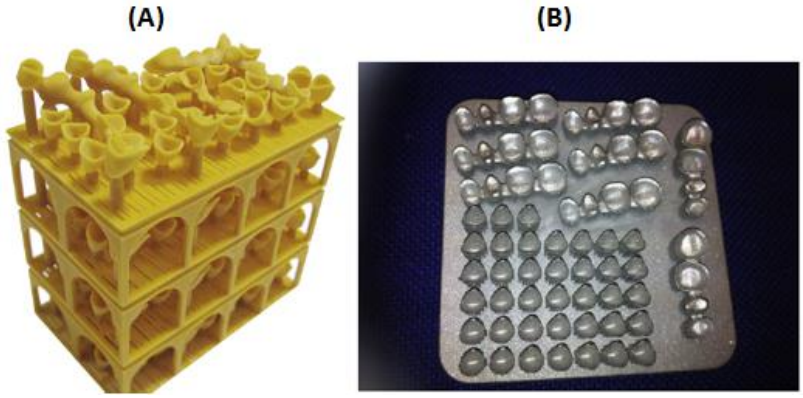

Figure 11. (A) Investment casting model in resin produced by Envisiontec. (B) Dental restorations made using the new Concept Laser Mlab using metal laser melting system. Adapted from [32]

1.3.2.1 Robocasting

Robocasting, depicted in Table 5, is an extrusion filament-based 3D printing process that emerged as a distinct AM over the years. [42], [43]

Robocasting is a rapid prototyping (RP) technique that allows freeform fabrication of dense ceramics and composites [44], by assembling geometries in a layer-by-layer process. This technique uses computer-controlled extrusion of colloidal pastes (also named slurries, gels, or inks) onto a flat substrate without additional molds or tooling. Robocasting acts by strategically print material in order to evolve three-dimensional (3D) structure instead of removing the unwanted material from a given stock by machining. The printing of the layers has some specific instructions based on the 3D computer model of the structure (*e.g.*, assembled using computed tomography (CT) scans, point clouds from optical scanning, or stereolithography (STL) files). When the 3D model is created, the software slices it in stacked layers, designing then a sequence of print operations to build the layers one above the other. This approach has had success in the assembly of various structures with applications in several areas ranging from electronics to bone scaffolds. It is also a process that has some potential advantages over CAD/CAM systems due to its ability to "print" with multiple materials at one time as well as create graded structures. Its capability to spatially grade composition and/or microstructure (*e.g.*, porosity) to meet specific designs or needs, without requiring a previous mold confers another advantage over CAD/CAM systems. [45]

The process starts with the robocasting ink, which is usually an aqueous paste of ceramic particles inserted into a pattern for a syringe. The paste is extruded as a continuous filament at a controlled rate through a nozzle attached to the syringe, as shown in Figure 12. The ink requirements demand that it must flow through the nozzle with modest pressure, retain the desired shape after deposition, dry with minimal shape change after printing, and sinter to high density.

Doubtless, and as previously mentioned, robocasting is a very flexible technique with regard to the range of materials that can be printed. However, it is somewhat limited in the shapes it can form. The pieces will always have step edges due to the layerwise nature and supports must be printed to allow significant overhangs or large spanning elements. The size of the edges is defined by the radius of the printed filament, typically being 100 – 250 μm, while other techniques such as stereolithography may reach one-fifth that size. The real advantage of robocasting lies on the mechanical quality of the material produced and the flexibility of the technique to print different materials, which allows internal morphology, shape, distribution and connectivity to be controlled more accurately. [43], [45]

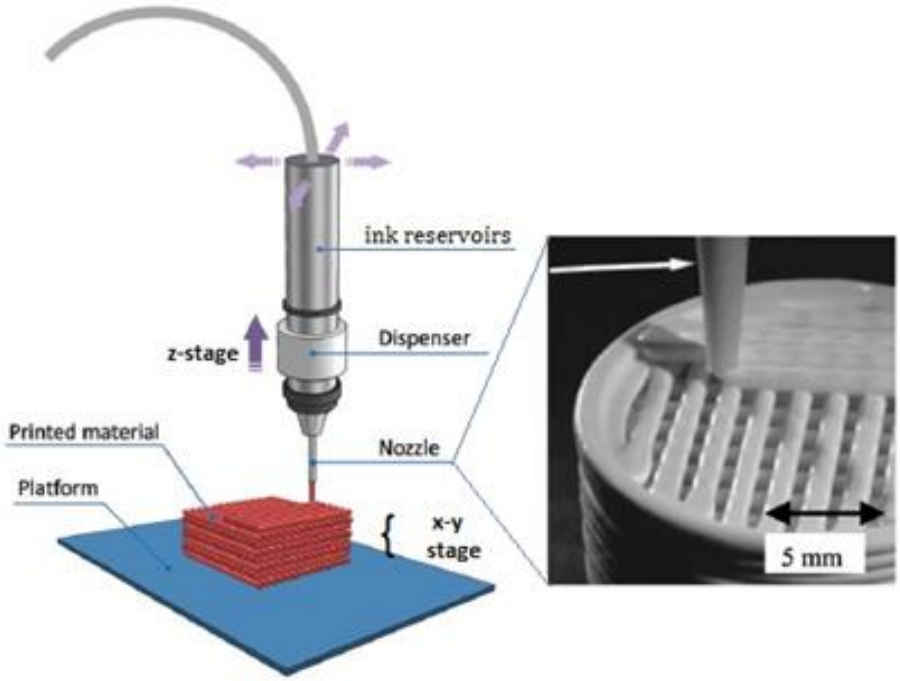

Figure 12. Schematic diagram of robocasting (direct ink writing). A material dispenser connected to a computer-controlled robot, scans across the building platform, depositing the ink material in a layer-by-layer manner. Adapted from [37], [42]

In this LDM technology for ceramic materials, highly charged colloidal slurries or suspensions are generally formed by a mixture of ceramic powder, water and additives (which act as chemical modifiers). This paste exits from an extruder head through an orifice, whose position is controlled by the material being deposited in thin sequential layers on a base, which may or may not be heated. [38]

1.3.2.1.1 Essential parameters for the robocasting materials

Robocasting offers a range of different materials that may be printed, from bioactive ceramics such as hydroxyapatite and *β*-tricalcium phosphate to dental ceramics such as aluminum oxide (Al_2O_3) and zirconium dioxide (ZrO_2). [43]

The properties and composition of the paste are considered as the most important factors for robocasting. The inks (or paste) should be free of air bubbles and homogeneous, contain a high volume fraction of ceramic powder and flow properties suitable for extrusion, and still be capable of maintaining their shape after printing. An ink should be highly shear thinning to allow extrusion through fine nozzles, and also retain a degree of strength and stiffness to be self-supporting following printing. This stiffness and strength equates to a large elastic component of the ink's viscoelastic response. Aqueous inks are also preferred due to their simplicity, lower toxicity, lower cost, and slower drying, while low concentrations of organic are desired to allow rapid burnout and high densities. Various approaches have been explored to satisfy each of these criteria, such as very high solids loading pastes which dry during printing, polymer-solvent based inks dependent on solvent volatility, and colloidal ceramic suspensions where the particles interact by van der Waals forces to form a weak network. [43]

Thus, for the success of the robocasting process in the production of a material, it is required a synergistic control of:

- paste viscosity and rheology;
- percent solids in the ceramic powder suspension;
- dispensing rate of the slurry through the orifice;
- drying kinetics of the dispensed bead of slurry, which determine the optimum build parameters;
- computer code for optimal machine instructions.

When a proper balance of these variables is achieved, the robocasting can be used to make intricate ceramic bodies that sinter in relatively strong, dense and defect free parts. [44]

1.3.2.1.2 Rheological behavior

Depending on their viscosity behavior as a function of shear rate, stress, deformation, and others, fluids can be characterized into different categories. Fluids obeying Newton's law where the value of viscosity is constant are known as Newtonian fluids. In addition, if viscosity is constant the shear stress is linearly dependent on velocity gradient. In turn, fluids in which the value of viscosity is not constant are known as non-Newtonian fluids (*e.g.*, colloidal suspensions of particles with flexibility and shapes that can form temporary bonds between them). These categories are based on the relationship between shear stress and the velocity gradient (rate of shear strain) in the fluid. These relationships can be seen in the figure below for some categories. [46]

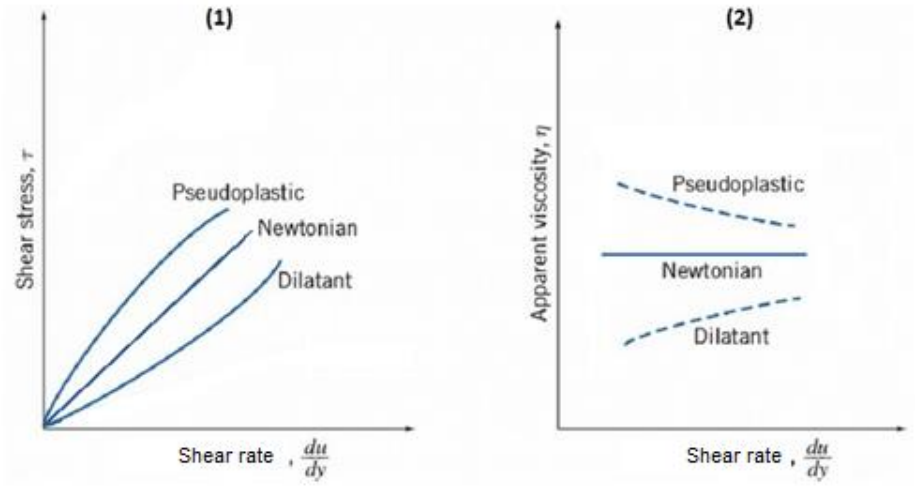

Figure 13. (1) Graph of the shear stress as a function of the shear rate. (2) Graph of the viscosity as a function of the shear rate.

Pseudoplastic fluids, those whose apparent viscosity decreases with increased stress are particularly interesting for robocasting since they have the ability to flow through small holes at modest shear rates. Unlike other free-form manufacturing techniques, robocasting does not require organic polymerization reactions or solidification of a polymer melt for solid transformation. Robocasting is based on the rheology of the deposited pulp and the partial drying of the individual layers, so that it is possible to maintain the structural integrity while constructing a component.

Summarily, a robocasting ink must satisfy the following criteria [44]:

- It must be pseudoplastic enough to be easily processed;
- After dispensing, it must be mounted in a non-fluid mass;
- It must be able to "accept" multiple layers without defects to form a uniform mass.

1.3.2.1.3 Solid contents in the ceramic powder suspensions

Typical ceramic powder suspensions have a relatively monosized distribution and their average particle size is in the range of several microns. These type of ceramic powders, which are dried from a dispersed slurry, typically have a consolidated structure which is approximately 65% of the theoretical density. [44]

For this technique of robocasting, the character of flowable slurries with solids loading just below the consolidated density is of extreme importance. Figure 14 depicts schematically the behavior of a typical dispersed alumina powder slurry. [44] At low solids loadings, dispersed suspensions have very low viscosity and are rheologically Newtonian. In the present case, at about 40% by volume of solids, even though the viscosity is still relatively low, the slurries begin to exhibit a pseudoplasticity shear-thinning behavior. As the solids content approaches 60% by volume, both inter-particle interactions and collisions begin to become dominant. In this case, the viscosity begins to increase appreciably, and the rheological

behavior becomes highly shear thinning. At approximately 63% by volume solids, the mobility of the particles becomes restricted and the slurry blocks in a dilating mass.

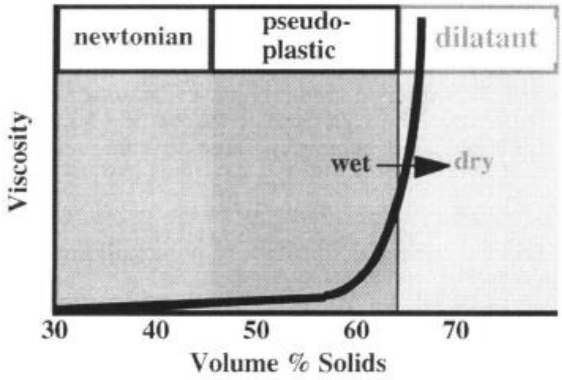

Figure 14. Scheme showing typical viscosity versus volume percent solids behavior for dispersed alumina suspensions. For ideal robocasting, work close to the dilatant transition. [44]

The pieces are typically constructed on a heated platform between 40 and 60 degrees Celsius to aid the pseudoplastic transition to dilatant, which in turn must closely follow the build speed in order to maintain structural integrity for thick parts. The drying rate is still an element to be evaluated, in the sense that if it is very slow, the pseudoplastic transition to dilatant is delayed and the accumulated weight of several layers eventually exceeds the yield stress of the pseudoplastic layers, a condition that can induce slumping and the creation of non-uniform walls. On the other hand, if the drying rate is too fast, warping, cracking and delamination may occur. [43], [44], [47]

In this perspective, it is recommended to robocast with slurries with solids loadings close to the dilatant transition, so that with a minimum drying a robocasted layer becomes structurally sound and a base upon which more layers can be deposited. [44]

1.3.2.1.4 Addition of dispersants and other additives

The stabilization of a suspension with respect to flocculation is determined by the forces of attraction and repulsion between the particles, which depends on their physicochemical characteristics and the particle-solvent interface. This stability is achieved when the repulsive forces are large enough to overcome the attraction forces. To obtain a stable suspension dispersants (deflocculants) are used, which, when adsorbed by the particles, increase the magnitude of the repulsion.

Dispersion of colloidal particles, with sub-micron and nanometer size, is a prominent issue in many industries, including ceramics processing. Dispersion is achieved by addition of certain reagents which adsorb onto the particles thereby increasing the interparticle forces to overcome aggregation.

Manipulation of the interparticle interactions (solid-solid and solid-liquid interactions) may allow the control the rheological behavior, providing an approach to optimize the suspension properties. [48]

In this perspective, the optimization has as prerequisite: a well dispersed slurry with high solids loading and is a preferred route to obtain near net shape components with a homogeneous and defect free structure. The use of polyelectrolytes, such as Disperx N40 [49] and Disperx A40 (sodium polyacrylate), Dolapix C64 and Dolapix C75 (ammonium salt of polymethacrylic acid) [48]–[50], and others, to promote the stabilization of suspensions against flocculation has been one of the most widely used alternatives in the ceramic industry, although several variables may affect the surface chemistry of particles including pH, type of dispersant, impurities, solvent, ionic strength and others. [48], [51] In addition, several organic additives, can be added to the suspensions in order to optimize the printability. These additives, which are all miscible with water, are commercial humectants that prevent clogging and drying, and are chosen according to the material safety data sheets of several commercial inks. [49] Ethylene glycol, ethanol, urea, C-Caprolactam, 1,6-Hexanediol, Poly(vinyl alcohol), and others, are examples of some of these organic additives. [38], [49]

In this way, robocasting focuses generally on the extrusion of highly loading ceramic pastes which are typically 50 – 65% by volume of ceramic powder, < 1% by volume of organic additives and 35 – 50% by volume of volatile solvent (usually water), although dispersants may optionally be used. [44], [45] However, other compositions with higher content of solids may be considered in specific cases, to optimize the processing of the materials.

Zirconia suspensions studies

In recent years, solid free-forming of ceramics has been a subject of intensive research [49] and more materials have been developed. Some materials characteristics should be taken into account regarding restorative dental applications, such as mechanical resistance (mainly strength, wear and toughness) and correspondence of optical properties such as shade and translucency to those of natural teeth. The recent use of high strength zirconia in dentistry industry has increased the spectrum of applications of this ceramic material, leading to the manufacture of ceramic crowns. [52] In addition, while in the conventional method a block of zirconia is processed, in 3D printing a suspension of ZrO_2 particles is used. Understanding the response of zirconia suspensions to processing can lead to more reliable methods of fabricating ceramics.

Colloidal suspension of zirconia particles by addition of suitable dispersants has also been studied widely. [49], [53] Typical dispersants which have been shown to disperse zirconia include Tiron, Aluminon, ammonium polyacrylate, polymethacrylic acid, polyethyleneimine, and diammonium citrate, 2-propenoic acid and a metalorganic polymer, Titron X-114, Triammonium citrate, Dispex A40, and Dolapix CE 64. These dispersants adsorb on to the particles thereby increasing the surface charge and hence the interparticle forces, which in turn leads to a stable dispersion. [48]

However, studies reported for robocasting of zirconia are rare. Erwin Peng et al. studied the robocasting of dense yttria-stabilized zirconia structures, where a suspension with low solid YSZ content (<38 vol%) was readily shaped into complex structure and sintered to dense part while retaining its original morphology without any warping, crack or deformation. [47] Nelson R.F.A Silva et al. reported the evolution of a CAD/CAM process where ceramic pastes of alumina and zirconia were deposited in a layer-by-layer sequence to build up crown structures by robocasting. Alumina and ZrO_2 (Y-TZP) powder were dispersed in water, using ammonium polyacrylate. In this work, a viscosifying agent named hydroxypropyl methylcellulose were also used, as well as a counter polyelectrolyte (polyethylenimine), in order to gel the slurry. This project resulted in pieces with a rough surface finish, so they concluded that it is necessary to improve the automation of nozzle alignment for accurate support material deposition. [45]

As a challenging job of dental restoration production, this project involving the optimization of zirconia pastes for robocasting is totally innovator.

Chapter 2 – Experimental Procedures

In this study, zirconia-based pastes for robocasting were developed and characterized, trying to meet the requirements described previously.

2.1 Materials

Zirconia powder containing 5.5 wt% Yttria (3 mol%) was purchased from Zircomet (Lot No. 131201) as a chemically precipitated white powder or granule. The specifications, according to the supplier, were as follows: purity>94.0%, BET surface area of 10–20m^2/g and particle size (d50) of 150 nm. Typical engineering performance data is also listed in Table 6.

The commercial polyelectrolyte Dolapix CE64 was ordered from Zschimmer and Schwarz (Germany), and was used as a dispersant. Its chemical structure is given in Figure 15 and other characteristics of the polyelectrolyte are listed in Table 7. Deionized and distilled water was used in the study, and the pH adjustments were done using NaOH.

Figure 15. Yttria Zirconia powder sample (left) and Dispersant Dolapix CE64 (right).

Table 6. Typical Engineering Performance Data for Yttria Zirconia [54]

Density	6.04 g/cm^3
Porosity	0 %
Tensile Strength	500 MPa
Compressive Strength	>2000 MPa
Young's Modulus of Elasticity	205 GPa
Hardness (Vickers Hv0.3)	1350 Kg/mm^2
Maximum Use Temperature	1000 ºC
Fracture Toughness K¹C	8.0 MPam½

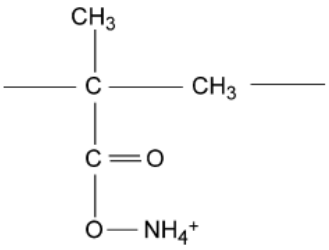

Figure 16. Chemical structure of the dispersant Dolapix CE64.

Table 7. Characteristics of Dolapix CE 64 dispersant.

Appearance	Yellowish liquid
Active matter	Approx. 65%
Solubility	Water-miscible
Density (20°C)	Approx. 1.2 g/cm^3
pH (original)	Approx. 7
Residue on ignition	Max. 0.1%

A paste based on zirconia was also supplied by the partner Centro Tecnológico da Cerâmica e do Vidro (CTCV), whose composition was achieved by extrapolating the optimization (made by a master thesis student [38]) of an alumina-based paste. This paste will be referred to as Paste B or Sample B and its composition is given in Table 8.

Table 8. Composition of Paste B.

		Raw materials	**%wt**	**Function of added materials**
Paste B	Zirconia 80 – 82 wt%	PVA (polyvinyl acetate)	5(*)	Plasticizer
		Deionized water	2	Solvent
		Citric Acid	>1,<3 (**)	Dispersant
		Powdered Sugar	10	Binder

(*) solution with a concentration of 20%

(**) solution with a concentration of 10%

PVA was selected as a plasticizer since it was evidenced that it softens the mixture before it cures, making it more workable without affecting the final properties of the final product. Citric acid was used as a dispersant, since it is known as dispersant for aqueous alumina suspensions. [38] Powdered sugar

was also used, which performs two functions: binder and rheology modifier during the formation and processing of ceramic pastes. [38], [55]

Commercial zirconia, which is a block of 5Y-TPZ containing 8.80 wt% Y_2O_3 (5 mol%), was purchased from Ivoclar Vivadent. This material is commonly used to produce dental restorations by SM, so it was used for comparison purposes.

2.2 Methods

2.2.1 Preparation of suspensions

Suspensions were prepared by mechanically mixing different proportions of zirconia powder in deionized-distilled water. These suspensions were stirred for about 30 min with a magnetic stirrer, and pH adjustments were accomplished with 0.2 M NaOH to obtain pH 8 (as reported in literature [48] for this dispersant). A fixed solid loading of 60 wt% was firstly used. Once the amount of dispersant that must be added (recommended by the manufacturer) ranges between 0.1% to 0.5% of the solids content of the mixture, suspensions having different levels of Dolapix CE64 were prepared in a slightly wider range, 0.1% to 2%, in order to determine the concentration at which a minimum viscosity is obtained. In order to study the effect of dispersant, and as suggested in the literature [48], Dolapix was added after the pH adjustments were done. Calculations of the amounts of Dolapix CE64 to be added were based on density. Detailed information about the components and dispersant concentrations (relative to the solids content in the suspension) used is reported in Table 9 and 10.

Table 9. Raw materials of the Zirconia paste prepared for robocasting.

Steps of slurry preparation		**Raw materials**	**Function of added materials**	**Density (g/cm^3)**
Zirconia Paste	Suspension	Zirconia powder	Ceramic	6.04
		Deionized-distilled water	Solvent	1.00
		Dolapix CE4	Dispersant	1.2

After selecting the ideal concentration of dispersant, *i.e.*, the one from which results the lowest viscosity, the amount of dispersant was fixed and the content of solids increased. For this, the paste with 60 wt% solids (which corresponds to 20 vol%) was concentrated by evaporation: it was kept at about 50 °C in an oven, for different periods till 48h, in order to evaporate water content. Then, suspensions of 70%, 80%, 90%, 91% and 92% in solids were obtained, for which viscosity measurements were also performed. It was not possible to obtain more than 92 wt% solids (which corresponds to 65 vol%) since, from this value, the paste was no longer homogeneous, presenting solid parts.

At the same time, it was also prepared a suspension with 90% in solids content, directly from the mechanical mixing of the components without involving evaporation of water.

The zirconia suspensions were left to rest at room temperature in closed vessels until the next day, to perform viscosity measurements.

2.2.2 Rheological measurements

Rheological measurements were made to study if the pastes were adequate to be used in robocasting, *i.e.*, if they presented pseudoplastic behavior.

The rheological properties of the zirconia suspensions were measured using a Haake Mars Modular Advanced Rheometer System of cone and plate (C35/2° Ti L). Liquid paraffin was deposited over the system to ensure that the suspension did not undergo evaporation during measurement. During these measurements, the suspension temperature was kept constant at 20 ± 0.1 °C by a thermostat. The viscosity measurements were performed as a function of the shear rate at different concentrations of the dispersant. A range of shear rates was employed (30 points from 0.1 to 150 s^{-1}) and measurements were made over a period of approximately 30 s at each shear rate. The measuring program was repeated three to five times for each sample to check reproducibility.

In turn, the rheological properties of the paste B were measured using a parallel-plates system (PP20 sensor), applicable to materials with very high consistency. The previous parameters remained constant.

Figure 17. Haake Mars Modular Advanced Rheometer System. [56]

Figure 18. Rheological measurements of zirconia suspension on Haake Mars Modular Advanced Rheometer System, located at Instituto Superior de Agronomia.

2.2.3 Preparation of the specimens

Firstly, it was attempted to simulate the extrusion involved in the robocasting using a syringe with a needle having an internal diameter of about 0.5 mm. No needle was used to Paste B (it was used a syringe having an internal diameter of about 2 mm). Spiral shape samples with approximately 6 mm diameter were produced and sintered. Sintering was carried out at a temperature of 1450 °C for 2h with a heating speed rate of 5 ºC/min and cooling in the furnace. After sintering, some of the samples were mounted and polished (as described below), to be observed under the optical microscope and to study its porosity, while others remained unpolished and were used for density measurements.

Since for further characterization samples with a regular shape and planar surfaces were needed, manual printing was used to fill silicon molds of rectangular plates, with the prepared pastes. To prepare the molds, small Perspex® parallelepipeds (acrylic; 3x1.5x0.5 mm^3) were placed in a petri dish and silicon was poured over them. Silicone 4514 T51 was left to polymerize with the parallelepipeds immersed, for about 24 hours. The parallelepipeds were removed from the mold, and the optimized zirconia paste (A), as well as paste B were extruded into the molds. The external surface of the samples was then gently flattened with a spreader and samples were left to dry at room temperature for more than one week. After drying and before sintering, the specimens related to the paste B were subjected to an intermediate process named debinding. This step was only necessary on B samples due to its high content of additives. The debinding process consists in the removal of binders and other additives with temperature (500 ºC, 2 h) in order to avoid cracks, distortions or contamination. The obtained specimens were then sintered with the same thermocycle referred above.

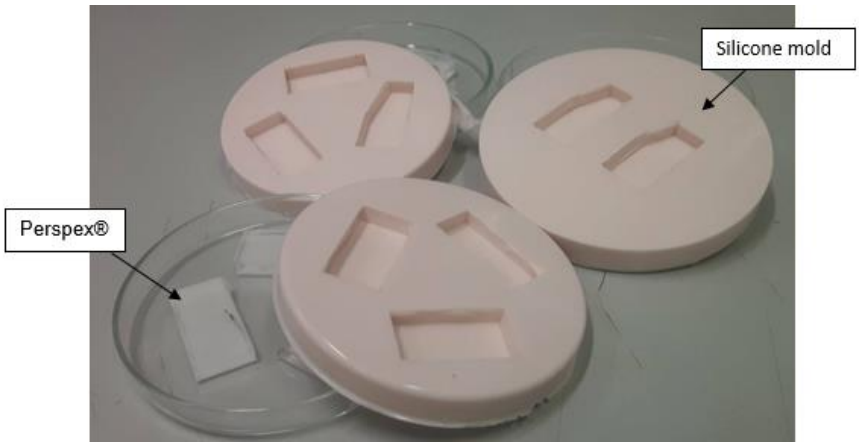

Figure 19. Silicone molds.

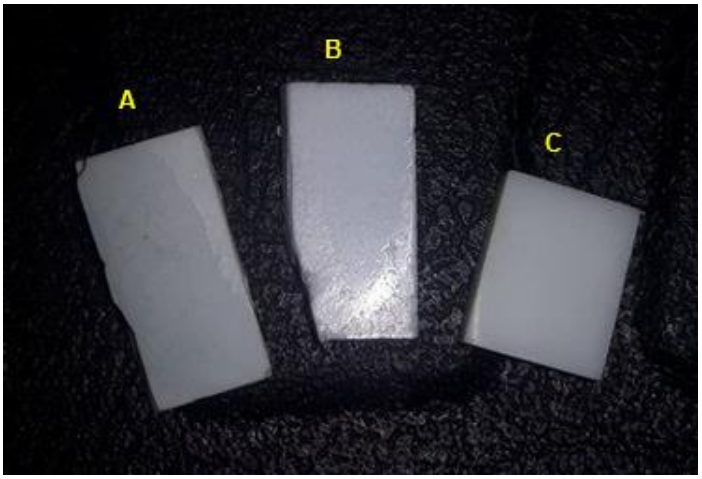

Figure 20. (A) Optimized paste; (B) Paste B and (C) Comercial samples

For polishing the sintered samples were previously mounted on resin phenolic green using a Buehler Simplimet 2000 Automatic Mounting Press. Then, the samples were polished with silicon carbide sandpapers accompanied with water with the sequential order of particle size of P600, P800, P1000, P2400, P4000. Some of them needed to be initially polished with P120 and P400, due to its irregular surface. After, in order to obtain a smooth surface, a polishing with 6 µm, 3 µm and 1 µm, grit diamond pastes was done.

Figure 21. Resin phenolic green and one of the obtained samples.

2.2.4 Samples characterization

The sintered samples of paste A (the optimized paste), paste B (provided by CTCV) and of commercial zirconia (samples C) were characterized concerning different properties.

2.2.4.1 Density measurements

Density measurements were performed on sintered specimens using the Archimedes principle. In Archimedes' principle the density of a solid body can be defined as the relation between the mass of the solid body and the mass of an equal volume of liquid. The deduced formula from the principle of Archimedes which was used is given by Equation 1. [57]

$$\rho_{object} = \left(\frac{m_C}{m_C - m_{AP}}\right) \times \rho_L \qquad (\mathbf{1})$$

where ρ_{object} is the density of the solid body, ρ_L is the density of the liquid (g/cm^3), which in this case will be water at room temperature, and m_C and m_{AP} are, respectively, the real mass and the apparent mass of the of the solid body. The calculation of the apparent mass was done by immersing the specimen in distilled water at 20 °C, using a support coupled to the balance, as shown in Figure 22.

In this way, it is possible to calculate the relative density (Equation 2), which is the ratio between the density (mass per unit volume) of a substance and the density of a given reference material. In this case it was used as reference the density of the nanostructured zirconia used to prepare the pastes, (6,04 g/cm^3).

$$d_{relative}(\%) = \left(\frac{\rho_{object}}{\rho_{ref}}\right) \times 100 \qquad (\mathbf{2})$$

The measurements were made on a Sartorius YDK03 balance, at Campus Tecnológico e Nuclear (CTN), which includes the proper density determination kit. For each sample, five weighing tests were performed outsider and inside water, so the densities used for each sample were based on the mean of these five essays.

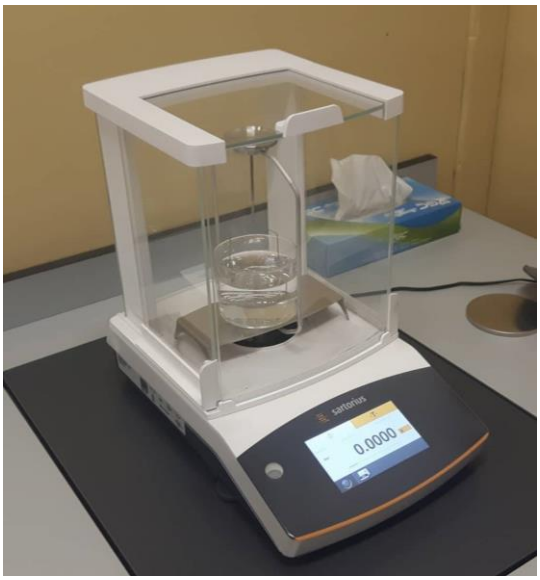

Figure 22. Sartorius YDK03 Balance with copled support for measurement of apparent mass

2.2.4.2 Porosity analysis

To evaluate the porosity of the samples, they were observed in the optical microscope after polishing. Some photographs were taken with resolutions of 5000X, 10000X and 20000X, not only to quantify the porosity but also to evaluate the distribution and size of the pores. This evaluation was done using the software ImageJ, which is a Java-based image processing program.

2.2.4.3 Surface morphology/topography

Topography

Sample surface topography can be studied using an atomic force microscope (AFM). [58] Atomic force Microscopy (AFM) is a versatile and powerful technique which allows the sample surface analysis, providing a three-dimensional image of the sample surface topography as well as various types of surface measurement data of a sample at the nanoscale. This technique has many advantages, including capability of extremely high resolution, and is a non-destructive technique where samples need to be minimally prepared (no need for sample treatment or coating). [7], [59]

The AFM principle is based on three main steps, surface sensing, detection and imaging, and involves four main components, a probe - flexible cantilever with a sharp tip, a piezoelectric scanner, an optical detection system and a feedback system. [7] In this method different types of interaction maps can be obtained, since there are several types of tip-surface interactions. In addition, distinct types of maps require different positioning of the tip: the tip may be scanned in contact with the surface (contact mode), scanned without contact (non-contact mode) or in intermittent contact (tapping mode).

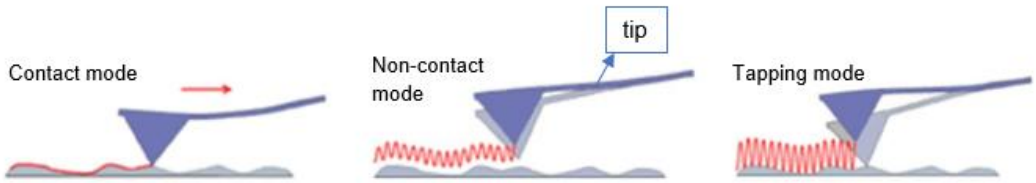

Figure 23. AFM Operational modes. Adapted from [59]

The operation mode chosen for the tests of this experimental work was the “contact-mode”, where the tip is simply moved across the surface, allowing the measure of the surface roughness. The topographical measurements of the zirconia samples surface were carried out using an atomic force (AFM) Nanosurf Easyscan2, at Instituto Superior Técnico. Topographical images were obtained through contact mode at room temperature with an applied force of 25 nN and at a scan rate of 1.2 Hz, using silicon probes (PPP-CONTSAuD-10, force constant 0.01-1.87 N/m). The software WSxM 5.0 Develop 4.0 was used to process all scanned images data and analyse the surface roughness. All topographic AFM images are presented in a color scale which represents the Z height.
One sample from each group A, B and C was analyzed. From those samples, up to three randomly selected regions of interest were scanned in order to calculate the average roughness value R_a (nm). Images of 20 μm^2 x 20 μm^2 were obtained. It was considered the total area of the images for the calculation of the average surface roughness by exporting the data to Excel.

Morphology

Scanning electron microscopy (SEM) is a method for high-resolution imaging of surfaces which uses a multifunctional and complex microscope that allows the analysis of microstructure morphology by obtaining images with high magnification. [60] To obtain an SEM image, the incident electron beam is scanned in a raster pattern across the specimen’s surface and the emitted electrons are detected for each position in the scanned area by an electron detector. The intensity of the emitted electron signal is displayed as brightness on a display monitor and in a digital image file. By synchronizing the position in the image scan to that of the scan of the incident electron beam, the display represents the morphology of the sample surface area. Then, the magnification of the image is the ratio of the image display size to the sample area scanned by the electron beam. All samples need to be able to handle the low pressure inside the vacuum chamber since the SEM column and sample chamber need to be at a moderate vacuum to allow the electrons to travel freely from the electron beam source to the sample and then to the detectors. [60], [61]

In the present work, SEM images were taken to analyze the samples surface before and after wear and indentation tests. Specimen from each tested group was selected. The surface of each sample was recorded photographically at different magnifications to record the cracks from indentations. Prior to the SEM imaging, the samples were cleaned and prepared. For both imaging analyses the samples were

coated in a vacuum evaporator with a thin layer of gold in order to to increase the conductivity of the samples surface and also to prevent charges accumulation. The SEM used was a Field Emission Gun (FEG) SEM JEOL JSM-7001F. The SEM imaging and the gold deposition were done in the MicroLab, Electron Microscopy Laboratory of IST.

2.2.4.4 Wettability tests

Because mouth has an aqueous environment, hydrophilicity is an important surface property, known to considerably affect dental properties and performance. [62] In this way, wettability, which is a physical phenomenon that is closely related to oral structures, presenting all relevance for dental prosthetic materials in terms of surface characteristics in interaction with saliva, is an important parameter to evaluate. The wettability of a material by a liquid is assessed by measuring the contact angle, which is defined by the angle formed between the solid surface and the tangent to the liquid surface in contact with solid, in the intersection between a liquid, a solid and a gas.

Young's equation (Equation 3) describes mathematically the wettability phenomenon [63] and relates the contact angle (θ), with the interfacial tension between solid and vapour (γsv), the interfacial tension between the solid and liquid (γsl), and the interfacial tension between the liquid and vapour (γlv).

$$\gamma lv \cos\theta = \gamma sv - \gamma sl \qquad (\mathbf{3})$$

The surface is hydrophilic when it has a low contact angle (*i.e.*, surface wetting is high). When 0° < θ < 90°, the liquid wets the solid surface. On the other hand, the surface is hydrophobic when it has a high contact angle (above 90°). In this case, the surface wetting is poor, *i.e.*, when 90° < θ < 180°, it is considered that the liquid does not wet the solid surface. When θ = 180°, there is no adhesion between the two phases (*i.e.*, there is no wettability). [7], [63]

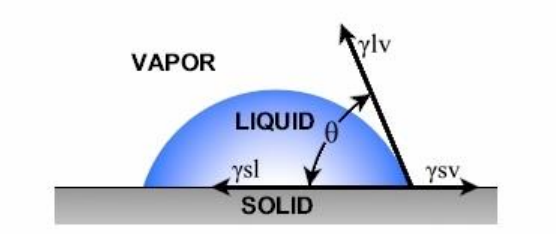

Figure 24. Interaction between a liquid droplet and a solid surface, on a hydrophilic surface. [63]

The wettability can be measured by various techniques, such as the sessile drop or captive bubble, where the contact angle is measured with a goniometer. The difference between the two lies in the fact that in the sessile drop method a drop of the liquid is placed on the top of the surface that is being analyzed, while in the captive bubble technique an air bubble is inserted below the surface, which is immersed in the liquid.

Under experimental context, the contact angle was measured by the sessile drop method using the goniometer system in order to evaluate the hydrophilicity of the sintered samples. Before wettability test was done, samples were cleaned with ethanol and dried in vacuum oven for about 5h. After, the zirconia samples were placed on the support surface. Using a micrometer syringe, a drop of distilled water was placed over the sample. The shape of the drop was visualized in several sequential images obtained by a video camera (JAI CV-A50) connected to a microscope WildM3Z and to a frame grabber Data translation DT3155, during a period of time of 1 minute and the experimental analysis was performed with the Axisymmetric Drop Shape Analysis Profile software. In each sample, 5 to 10 drops were placed (1drop=1essay), and for each type of sample resulted fourteen contact angles, from which an average was made.

2.2.4.5 Tribological behavior

Teeth wear may result in inefficient contact of the teeth during mastication and may lead to bad function and deterioration of the temporomandibular joint. [58] Dental surfaces are biotribological systems whose performance may be affected various mechanisms of friction and wear. [64] In this way, it is important to evaluate the tribological characteristics of the zirconia samples that will eventually replace the teeth.

The nanotribometer equipment was used in this work for that purpose. It includes three main elements, two optical fibers connected to the piezoelectric sensor, a cantilever (force transducer) and the counter-body that interacts with sample surface. During tribological tests, the counter-body is loaded into the sample with a precise known force. The relative movement between the two interaction surfaces induces deflection of the cantilever which is detected by the spring bars. The two optical fibers emit a beam of infrared radiation that is reflected by the two perpendicular mirrors allowing the measurement of vertical and lateral variations of the normal force and the frictional force, respectively. In this way, the system provides the coefficient of friction value (*i.e.*, frictional forces of relatively moving surfaces in contact). For the operation of this test, several characteristics were defined for setting up the nanotribometer through the Tribometry software (Microsoft Windows 2000/XP platforms) and handling the data.

In this work, a CSM nanotribometer was used, in order to obtain the friction coefficients of the produced materials and the commercial sample, and also to try to study the wear behaviour of the different samples. It was used as lubricant artificial saliva (prepared on the day through the recipe shown in Table 9, with pH=6.5). The counter-body used was a zirconia sphere of 3 mm diameter supplied by Technoball (hardness of 1350 HV, elastic modulus of 205 GPa), in order to simulate a zirconia/zirconia system. All

tests were carried out at room temperature under a constant vertical applied load of 100 mN, 1300 cycles (approximately 10 minutes), sliding distance of 1 mm/cycle and frequency of 2.12 Hz. InstrumX software (version 4.4) was used to acquire the raw friction test data that was subsequently processed and analyzed.

Table 10. Recipe for the artificial saliva, provided by [12].

Reagent	Concentration (g/L)
NaCl	0.600
KCl	0.720
CaCl2	0.166
KH2PO4	0.680
Na2HPO4	0.337
KSCN	0.060
NaHCO3	1.500

Furthermore, it is still relevant to analyze the contact between these two elastic solids. The relation of the deformation of the material with a normal applied force (F_N) in a spherical-plane contact was defined by Hertz in 1882 [65], as being:

$$F_N = \frac{4}{3} E^* . R^{1/2} . (R - d)^{3/2} \quad (\mathbf{4})$$

Where R is the ration of the sphere curvature, $(R - d)$ is the maximum deformation in the contact area and E* the elastic modulus which is dependent on the Young's modulus (E1, E2) and Poisson coefficients (v1, v2) of both materials in contact, which in this case is the same material. E* is given by: [65]

$$E^* = \frac{E_1 E_2}{E_2(1 - v_1^2) + E_1(1 - v_2^2)} \quad (\mathbf{5})$$

Since the contact area, A, is given by [65]:

$$A = \pi . a^2 = \pi . \left(\frac{3}{4} . \frac{F_N . R}{E^*} \right)^{2/3} \quad (\mathbf{6})$$

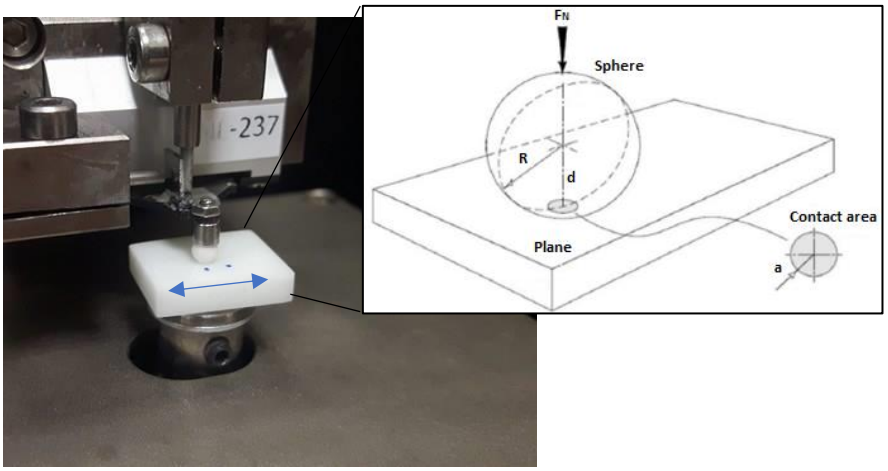

Figure 25. Tribological test on the zirconia commercial sample, regarding spherical-plane contact. Adapted from [65]

The maximum compressive contact pressure P_{max} applied across the contact area as an elliptic distribution in the surface is given by [65]:

$$P_{max} = \frac{3.F_N}{2.\pi.a^2} = \left(\frac{6.F_N.E^{*2}}{\pi^3.R^2}\right)^{1/3} \quad (7)$$

While the mean compressive pressure (P_0) is equal to $^2/_3$ of P_{max}, the shear stress τ_{max} is given by [46]:

$$\tau_{max} = 0.31P_{max} \quad (8)$$

Table 11 reports the Young's modulus (E1=E2) and Poisson coefficients ($\upsilon_1 = \upsilon_2$) of zirconia, in order to calculate the contact elastic component (E*). As previously mentioned, the normal force chosen for the tribological tests was 100 mN, so a value of $F_N = 0.1\ N$ was used to calculate the mean pressure applied across the contact area. The applied average compressive contact pressure obtained by applying the Hertz equation for elastic contact was 319 MPa. According to the literature [12],[66] this value is within the masticatory pressure (compressive pressure between 35 and 350 MPa, if it is considered an occlusal contact area of 2 mm^2), confirming the possibility of using this normal force in this system.

Table 11. Young's modulus and Poisson coefficient of zirconia. [54], [67]

Yttria Zirconia data	S.I
E_1, E_2	2.05 x 10^{11} Pa
υ_1, υ_2	0.31
R	1.5 x 10^{-3} m

2.2.4.6 Microhardness tests

Vickers hardness test is a mechanical test in which an indenter (shown in Figure 26) is forced into the test-piece surface under a defined force, held for a defined duration and removed. This method allows to measure the indentation hardness value which is obtained by measuring the depth or area of indentation left in the tested material. Thereby, the indentation diagonal lengths are measured, the mean result calculated, and this value then employed to calculate a hardness number which is equivalent to the mean force per actual unit area of indenter surface contacting the test surface. [29] Vickers Hardness is given by Equation 9:

$$HVF = 1{,}8544\,{}^{F}/_{d^2} \qquad (\mathbf{9})$$

where HVF is the Vickers hardness number at applied force F (express as the mass in Kg from which F is derived), and where d is the mean length of the diagonals of the indentation (expressed in mm). [58]

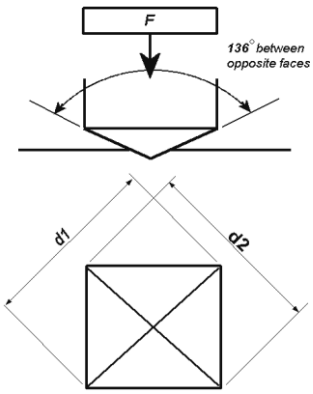

Figure 26. Square-based sharp pyramidal diamond indenter having specified face angles used on Vickers hardness. [29]

In this work, one sintered specimen of each group (A, B and C) were randomly selected to measure Vickers hardness using an indentation tester (HSV-30 Shimadzu model, from Instituto Egas Moniz). About five to six indentations were made on the polished surfaces using a loading mass of 1kg, 10kg and 30kg during 15 seconds, in five widely separated locations. Mean and standard deviation values were calculated. The values of average indentation diagonals were obtained from at least five readings in each sample.

Also, the corresponding crack lengths were measured from SEM micrographs. Fracture toughness of sintered materials was estimated using the three indentation methods described in [10] and [68], by several Equations:

$$K_{c,i} = \frac{H}{E} \times \frac{P}{c^{3/2}} \quad (\mathbf{10})$$

$$K_{c,i} = 0.016 \left(\frac{E}{H}\right)^{1/2} \times \frac{P}{c^{3/2}} \quad (\mathbf{11})$$

$$K_{c,i} = 0.0726 \times \frac{P}{c^{3/2}} \quad (\mathbf{12})$$

where $K_{c,i}$ is the indentation fracture toughness (Pa·m$^{1/2}$), H is the hardness in GPa, E is the Young modulus in GPa, *P* is the indentation load (*N*) and *c* is the median length (m) of the most severe produced crack in the corresponding indentation mark. The Young modulus shall be approached taking into account the porosity of the materials, *i.e.*, a value of $E=E_0(1–1.9P+0.9P^2)$. [69]

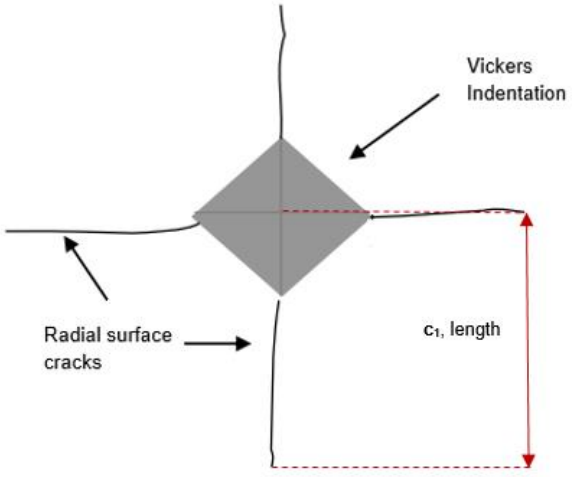

Figure 27. Indentation fracture. Adapted from [70]

Chapter 3 – Results and Discussion

3.1 Characterization of the pastes

Two different types of zirconia-based suspensions were studied in this work: one containing a dispersant polyelectrolyte and that was target of an optimization procedure (Paste A), and another one prepared by CTCV (Paste B) containing several additives.

In the first one, Dolapix was used as dispersant. Dolapix CE64 is a carbonic acid based polyelectrolyte and, according the manufacturer, is particularly suitable for deflocculation, due to the interaction between the bivalente functional groups of the additive and the surface charge of the ceramic particles. The paste optimization process involved the study of the influence of the Dolapix content, preparation methodology and solids content. The second one contained PVA, citric acid and powder sugar, which, as referred in section 2.1, acted, respectively, as plasticizer, dispersant and binder.

3.1.1 Paste A

3.1.1.1 Effect of the dispersant content

For the first type of pastes studied, the viscosity was determined as a function of shear rate at different concentrations of Dolapix (0.1 to 2%) for suspensions containing 60% solids, to optimize the amount of Dolapix that shall be added to the mixture. The obtained results are presented in Figure 28.

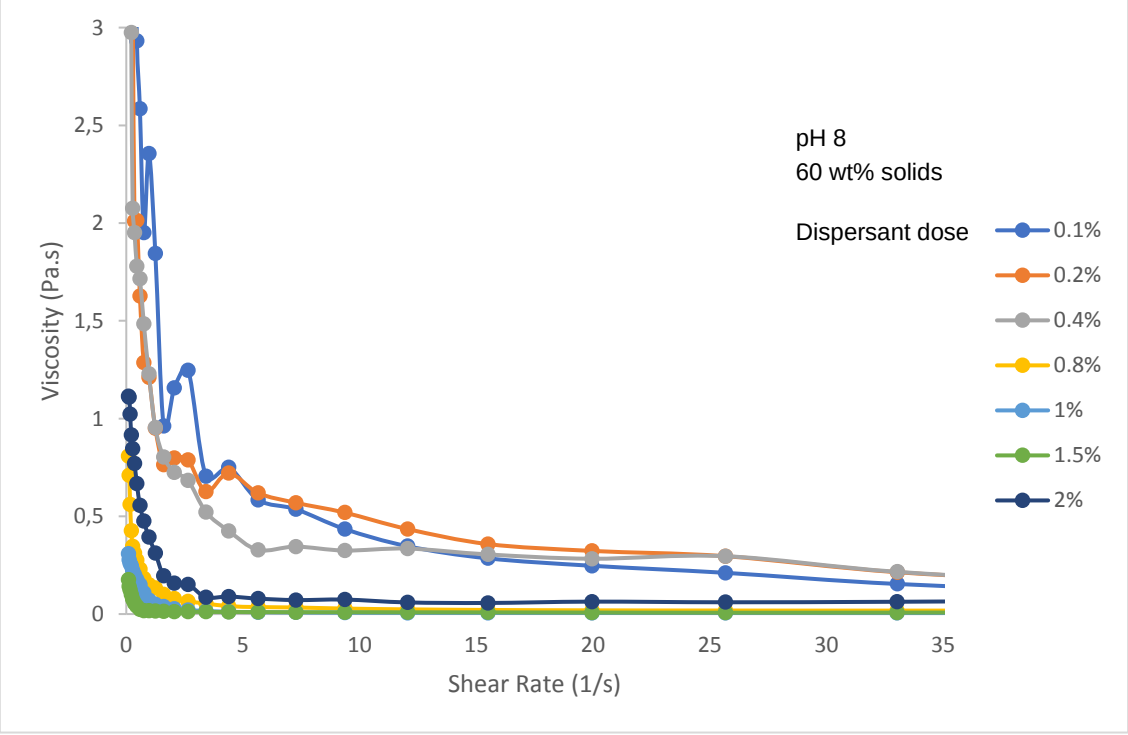

Figure 28. Viscosity as a function of shear rate for different amounts of Dolapix in 60%solids.

It can be observed that the viscosity decreases exponentially as the shear rate increases, for any added amount of dispersant. With 0.1% of Dolapix, the viscosity changes in an irregular way for low values of shear rate (< 5 s^{-1}), which proves that this concentration does not make the suspension to steadily flow, still being unstable. At concentration 0.2 and 0.4% a notable change is noticed, and the curves become more regular. The suspension is less viscous and flows more easily. From concentration of 0.8% forward, the peaks corresponding to the initial resistance to flow are quite smaller and the suspension starts to steadily flow. With the increasing of the concentration of Dolapix to 1% and 1.5%, viscosity values became quite low, there being practically no resistance to the suspension to flow. With 2%, the resistance to the suspension flow reappears.

Therefore, as the dispersant concentration increases till 1.5%, the flow resistance decreases. This can be explained by the adsorption of the Dolapix to the particle surfaces, which creates an electric double layer and provides electrosteric stabilization, considerably reducing the interactions between the particles and preventing them from forming agglomerates or a rigid network. In other words, with the addition of dispersant, the charge of the particles increases which keeps them dispersed. For the optimal electrolyte concentration, the zeta potentials of the neighboring particles lead to an ideal equilibrium between attractive and repulsive forces. For higher Dolapix concentration (2%), the viscosity increases because the particles diffuse layer becomes thinner when the electrolyte concentration increases. When the electrolyte concentrations become too high, the attractive forces predominate and the tendency to agglomerate increases.

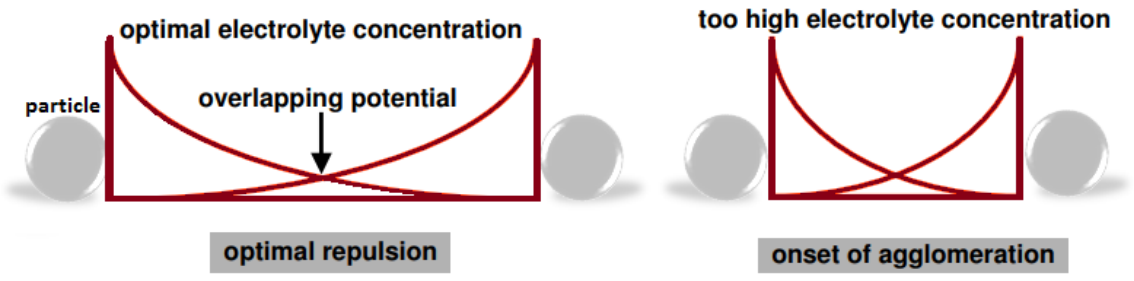

Figure 29. Overlap potentials of neighbouring raw material particles. Adapted from [71]

The obtained results indicate that the amount of Dolapix affects the flow properties of zirconia suspensions and that a higher shear rate is required to make the suspension flow.

Based on the data of Figure 28, several different shear rates were chosen to plot viscosity of zirconia suspension against the amount of dispersant. It is known that for the extrusion of ceramic pastes through a nozzle (as happens in robocasting), the overall shear rate distribution is not homogeneous, being zero in the center of the noozle and maximum at the noozle wall. Depending if the fluid is Newtonian or not,

a V or a U-shape shear rate distribution is observed, respectively, with values that depend on the nozzle diameter and printing speed. For a Newtonian fluid, Peng *et al.* [47], [72] determined that for a printing speed of 5 mm/s and a noozle diameter of 0.41 mm, the maximum shear rate is 31 s^{-1}. Shear rate values around 20 s^{-1} may be used as reference for the extrusion of ceramic pastes in robocasting. [73] Results are shown in Figure 30. It can be observed that to obtain a deflocculated dispersion, with the minimum viscosity, a content of dispersant between 0.8% and 1.5% must be used.

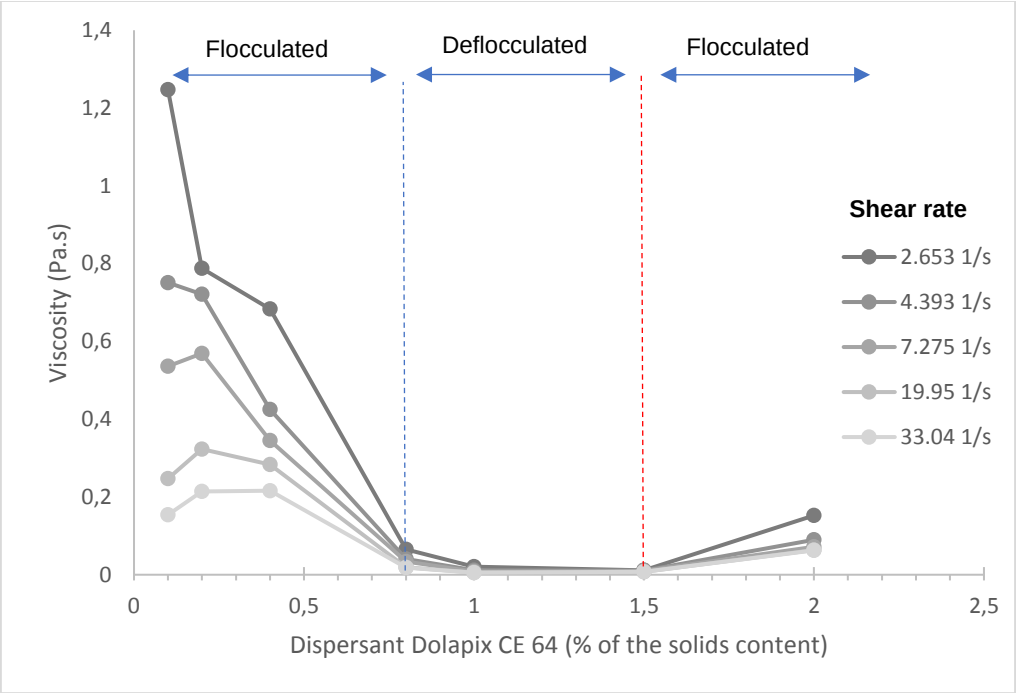

Figure 30. Viscosity in function of the amount of dispersant, for 60% solids.

In order to reinforce the data obtained from Figure 30 and reach the objective of discovering the concentration of Dolapix that allows to obtain a more stable dispersion (*i.e.*, a minimum of viscosity), it was necessary to study its rheological behavior in terms of consistency and flow rate. According to Newton's law, viscosity (η) is defined as the quotient between the shear stress (τ), expressed in Pascal (Pa), and the shear rate (γ), expressed in s^{-1}:

$$\eta = \frac{\tau}{\gamma} \tag{13}$$

In the case of non-Newtonian fluids or suspensions, the variation between the shear stress and the shear rate is not linear and can be related through the following equation, usually referred to as the power law:

$$\tau = k.\gamma^{n} \tag{14}$$

where γ is the deformation rate, k is the consistence (Pa.s^n) and n is the flow rate. The exponent, n, characterizes the behavior of the fluid which depends on the behavior of viscosity against shear rate. In Newtonian fluids, the viscosity depends only on temperature and pressure, where n=1. When n>1, the fluid has a dilatant behavior, that is, its viscosity increases with the shear rate, and if n<1, the fluid has a pseudoplastic or reofluidificant behavior (both non-Newtonian). [38], [46]

Since the fluid has a non-Newtonian behavior, in particular pseudoplastic (since viscosity decreases with shear rate), the power law is expressed in the general form of Newton's law (Equation 15), which is the simplest and most used to translate the (apparent) viscosity of non-Newtonian fluids.

$$\eta_a = k_0.\gamma^{n-1} \tag{15}$$

From the linearization of Equation 15 we obtain the logarithmic function (Equation 16), being possible to determine the value of n by the slope of the line and the k_0 by the ordinate in the origin.

$$log\eta_a = logk_0 + (n-1)log\gamma_a \tag{16}$$

The curves of viscosity presented in Figure 30 were then transformed to logarithmic scale and simplified, adjusting the power law only to the reofluidificant zone, through the line equation obtained as:

$$y = (n-1)x + \log(k_0) \tag{17}$$

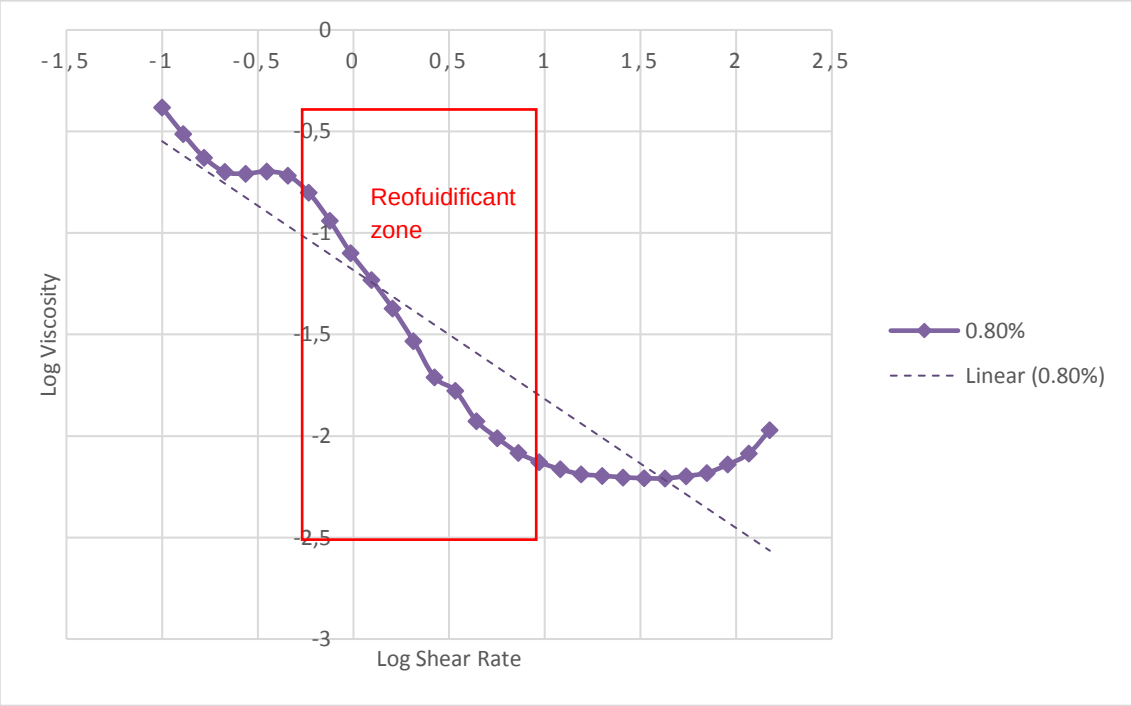

Figure 31. Logarithmic scale of viscosity as a function of shear rate, for 0.8% of dispersant.

Then, the effect of varying amounts of Dolapix on zirconia suspension consistency and flow rate is represented in Figures 32 and 33, respectively.

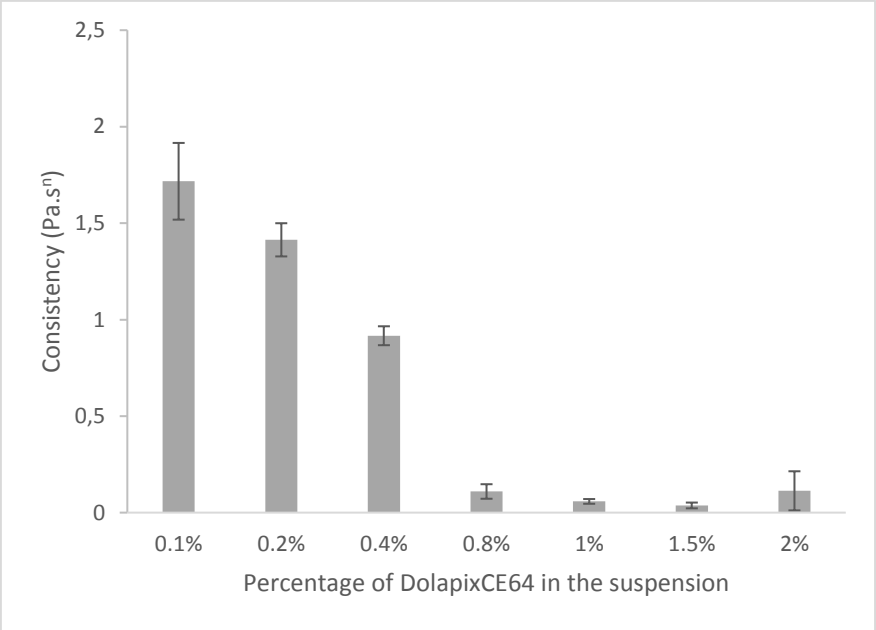

Figure 32. Average of the consistence for the different amounts of Dolapix.

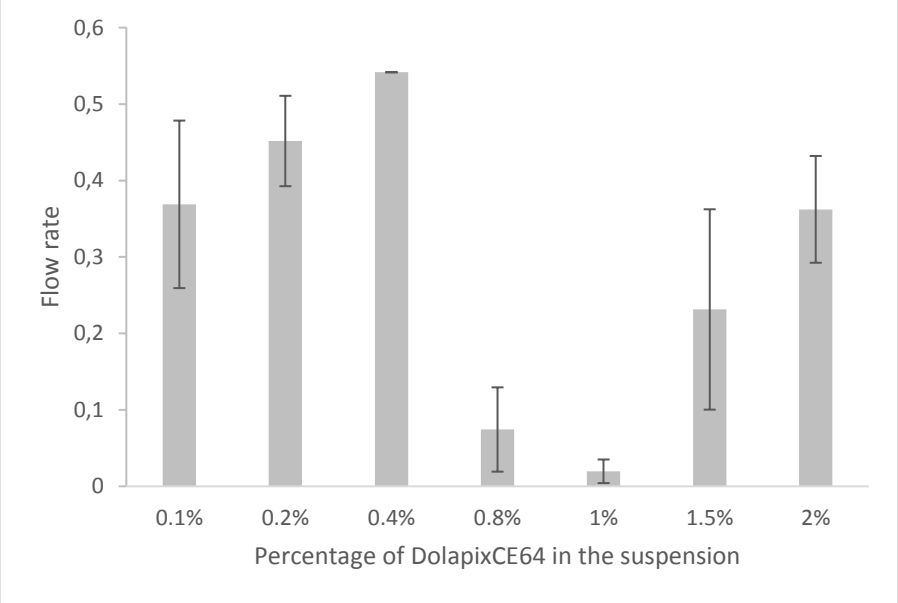

Figure 33. Average of the flow rate for the different amounts of Dolapix.

As can be seen from Figure 32, the consistency decreases as the concentration of Dolapix in the solution is increased to 1.5%, but slightly increases for 2%. Although the minimum value of consistency was observed at 1.5% (0.04 ± 0.01 Pa.s), this concentration of Dolapix leads to a much higher flow rate of

the suspension (Figure 33), with a great dispersion of results (0.23 ± 0.13). On the other hand, a minimum value of the flow rate was observed for 1% of Dolapix (0.02 ± 0.02). Since a content of 1% led to a value of consistency very close to the observed minimum, and for shear rates above 5 s^{-1} the viscosity of this suspension is consistently lower than the observed for 1.5% (all the experiments for 1% led to values lower than the observed for 1.5% – see typical curves in Figure 34, which is a magnification of Figure 28), it was decided to use 1% of Dolapix as the basis for the preparation of the suspensions of zirconia particles with higher solids content.

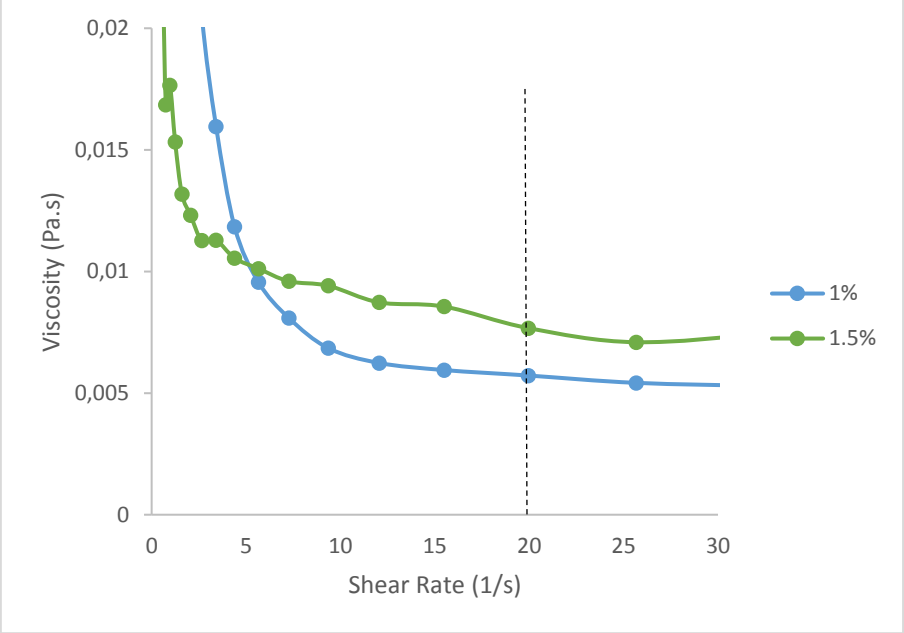

Figure 34. Viscosity as a function of shear rate for 1% and 1.5% of Dolapix in 60%solids. A typical value of shear rate for the extrusion of ceramic pastes by robocasting is pointed out (20 s^{-1}).

3.1.1.2 Effect of the preparation methodology

Two strategies were used to prepare the pastes with Dolapix: direct preparation with a high content of solids (90%) and increase of the solids content by evaporation (pastes with 60% of solids were heated to evaporate water and get mixtures with higher concentrations of solids). In both cases the previously defined optimal amount of Dolapix was used (1%).

The preparation of a suspension directly by mixing deionized and distilled water with dispersant in a large amount of solids resulted in a heterogeneous paste, filled with small aggregates (Figure 35). This happened because the amount of water with dispersant added was significantly less than the amount of zirconia powder ($10\%\ water\ /\ 90\%\ zirconia$), which causes Dolapix CE64 to be unable to homogeneously coat all particles of the paste. The agglomerates formed, permanent or not, besides influencing the rheology of the suspensions, can interfere in the packaging of the produced specimens

and, consequently, in their microstructure, making this paste improper for the final purpose of the work (3D printing).

Thus, agglomerates should be avoided, always seeking dispersed suspensions that, in addition to having a lower viscosity, ensure the homogeneity of the paste. For this reason, it is necessary that the dispersant involves all the particles to avoid sedimentation and consequent segregation of phases. Through the evaporation method, the concentration of solids may be increased allowing the paste to remain homogeneous and stable for a longer period of time. In fact, the initial low concentrations of solids allowed Dolapix CE64 to interact with all the ceramic particles of the fluid suspension, achieving a homogenous distribution, and enable an easy agitation of the suspension, which contributed to the breaking of eventual small aggregates.

Figure 35. Heterogeneos paste resulting from directly mixing 90% solids.

Figure 36. Homogeneous paste based on the evaporation of water.

3.1.1.3 Effect of the solids content

Zirconia based pastes with 1% Dolapix were prepared with different solid contents, by evaporation of a starting paste (ink) with 60% of zirconia. Figure 37 shows the relative viscosity vs. shear rate for the obtained suspensions over a range of solids concentrations between 70 and 92 wt%.

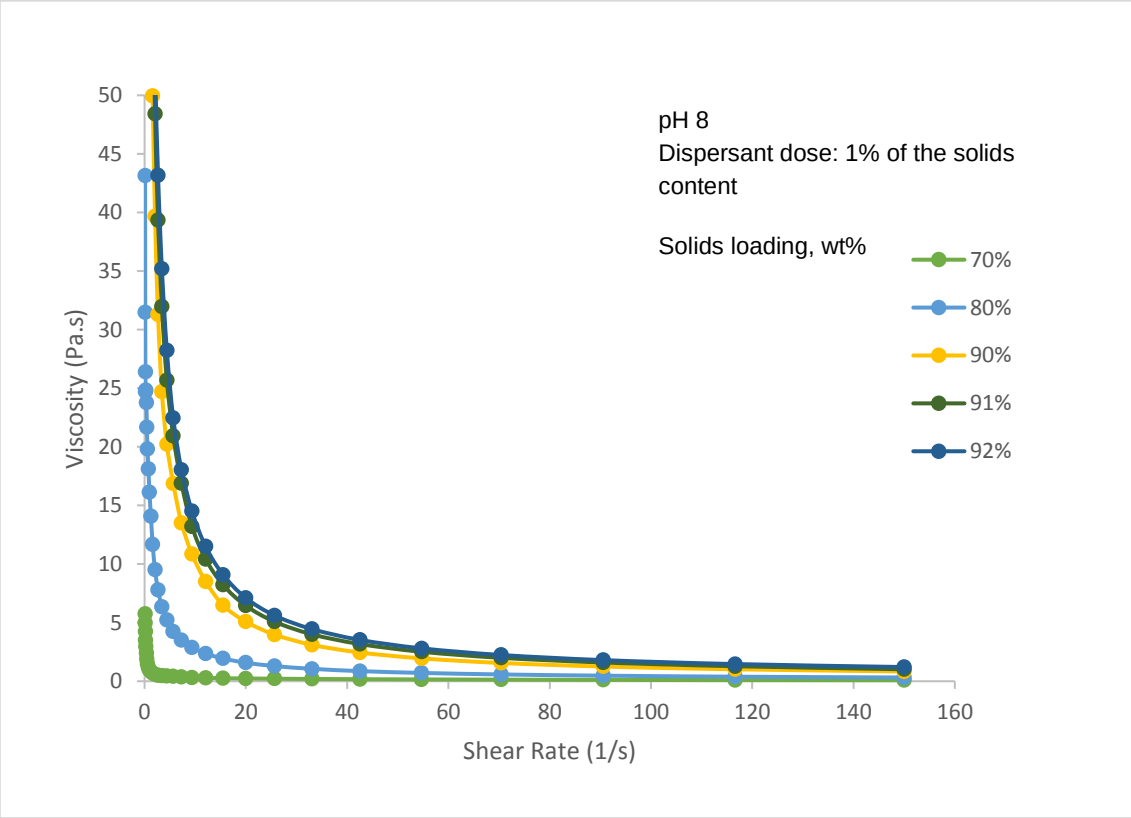

Figure 37. Viscosity as a function of the shear rate for different solids contents in pastes with 1% Dolapix.

As might be expected, at low shear rates, viscosity was found to increase with increasing solids loading, thus becoming more suitable to the purpose of the work. The decay in viscosity is exponential. Equation 16 was again applied, and the values obtained for consistency and flow rate are shown in Figure 38 and 39.

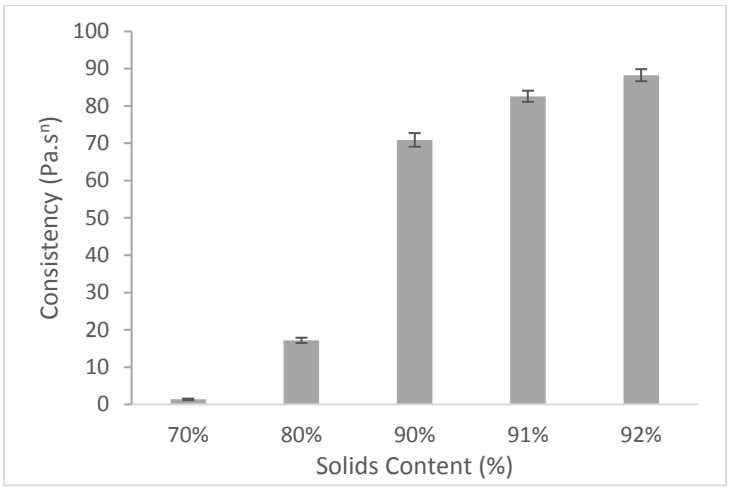

Figure 38. Average of the consistency for the pastes with different solids loadings and 1% Dolapix.

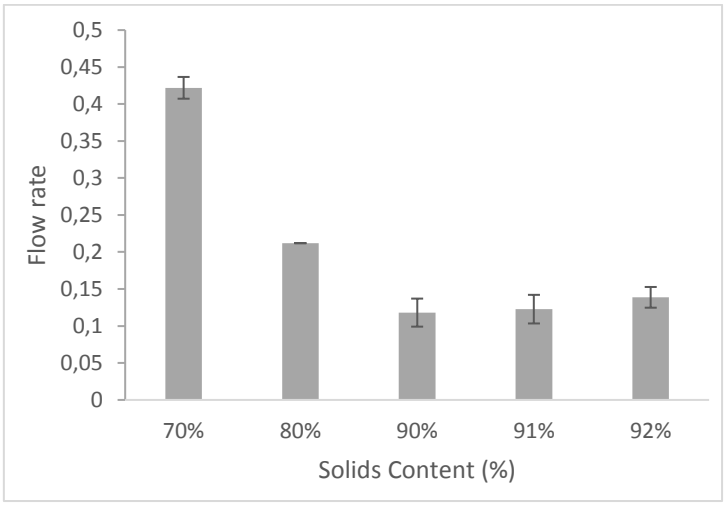

Figure 39. Average of the flow rate for the pastes with different solids loadings and with 1% Dolapix.

These results show that as the solids loading increases, the consistency of the paste also increases, presenting relatively higher values of consistency for solids loading greater than 90% (70.91 ± 1.83, 82.61 ± 1.49 and 88.26 ± 1.62 Pa.s for 90, 91 and 92% respectively). In addition, the flow rate tends to be much lower for zirconia suspensions with higher solids content, which demonstrates that pastes with >90% solids loading are more suitable for the purpose of this study. It should be stressed that, in section 3.1.1., the objective was to find a concentration of Dolapix that allowed to produce an ink with the minimum consistency and flow rate, to be used as starting point to obtain pastes with higher content of solids, through an evaporation process. However, here, the objective is different: it is aimed to obtain pastes with maximum consistency and minimum flow rate to enhance the printing process.

The viscosity was represented in function of the solids loading, at the same shear rates used previously (see Figure 30). As expected, in all cases the viscosity increases with the solid content. More, higher

shear rates lead to lower viscosities. It shall be underlined that all the studied pastes present a pseudoplastic behavior, as is recommended, to facilitate the printing process (see section 3.2.1.2).

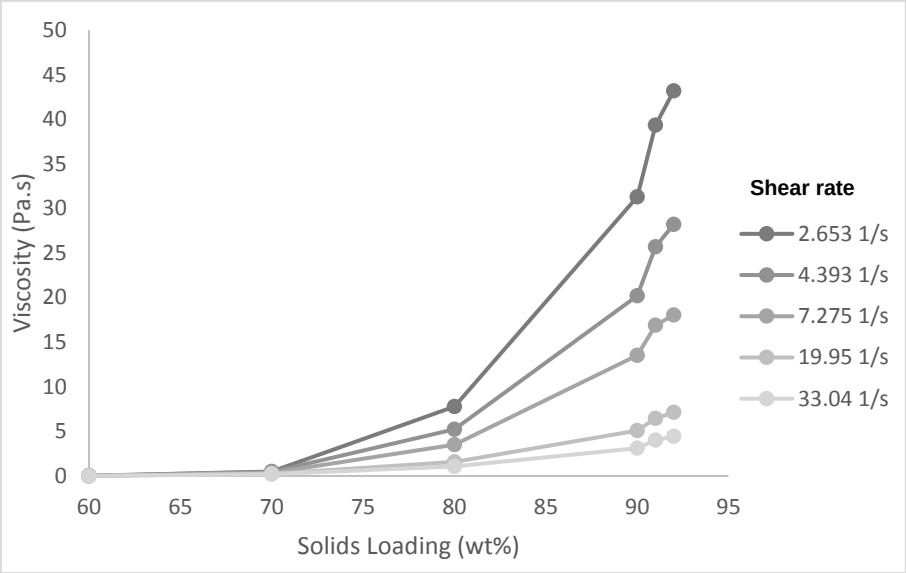

Figure 40. Viscosity versus solids loading behavior for zirconia slurries at 1 wt% Dolapix, at three different shear rates.

Taking into account the obtained results, further studies were carried with pastes containing 90%, 91% and 92% of solids.

3.1.2. Paste B

The results of the rheological measurements for paste B are shown in Figure 41.

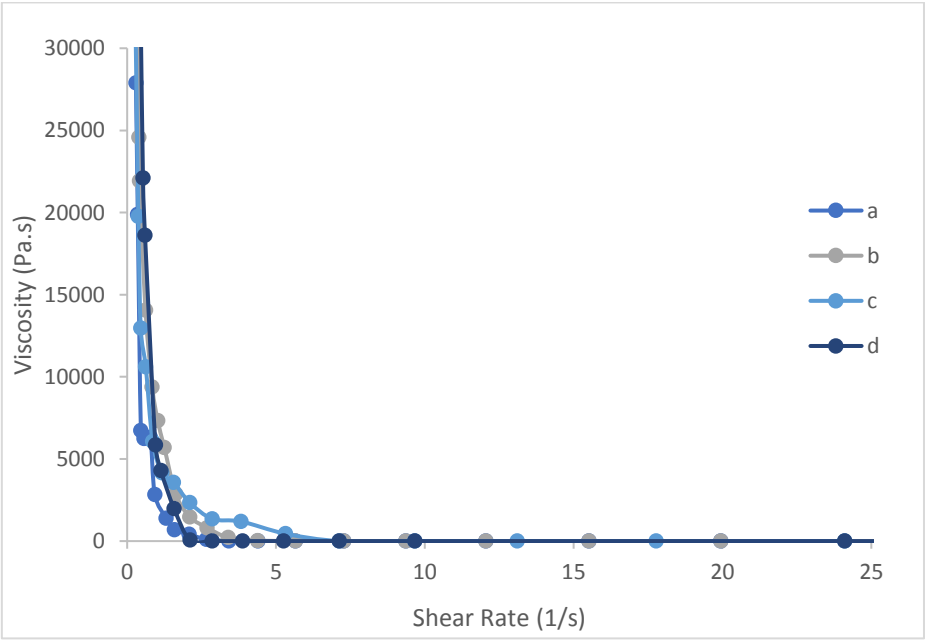

Figure 41. Viscosity as a function of the shear rate for Paste B (4 essays).

It can be seen from Figure 41 that the viscosity values for the paste B at low shear rates are quite superior to those found in the optimization process of Paste A. This means there is a great resistance to flow at low shear rates. The logarithmitization of the results led to curves with three distinct zones (Figure 42).

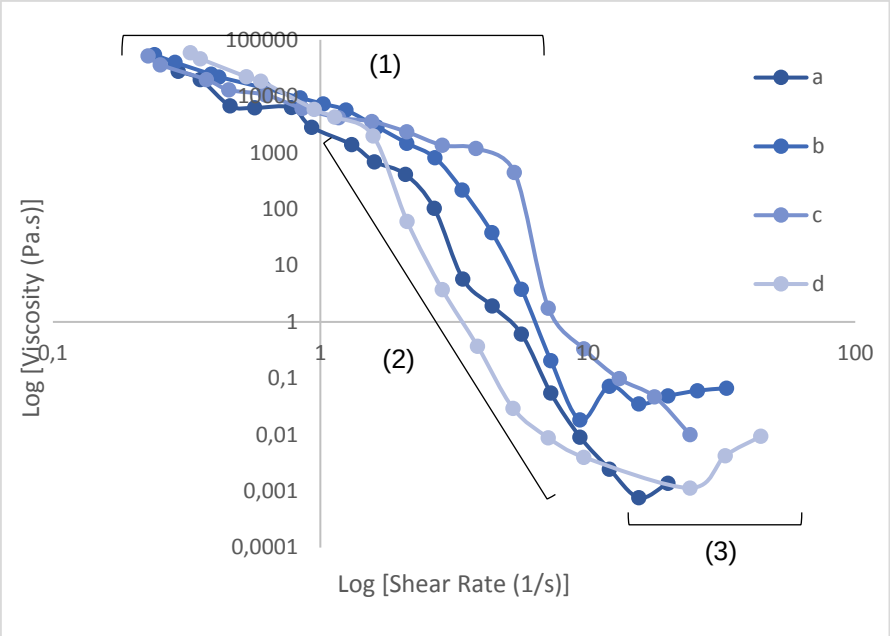

Figure 42. Logarithmic scale of viscosity as a function of shear rate.

A first reofluidifying zone, with a lower slope for low rates of deformation (1) another reofluidifying zone with a more accentuated slope (2) and a smaller zone that gives an idea of being a Newtonian plateau (3) were observed. It was not possible to apply the power law (Equation 14) to the reofluidifying zone, to determine the rheological parameters of the paste, since the value of n (flow rate) came negative, which does not have any physical meaning.

This problem could be overcomed by fitting other rheological models (*e.g.*, Cross or Casson) [46], that would imply a deeper analysis of the results, which is outside of the scope of this thesis.

3.2 Production of the specimens

Figures 43 and 44 represent the simulation of the *robocasting* extrusion of Paste A and and of Paste B, respectively, using a syringe system. In the first case, Pastes with 90%, 91% and 92% of solids were tested. However, due to the similarity of the obtained specimens, only images of 90% are shown.

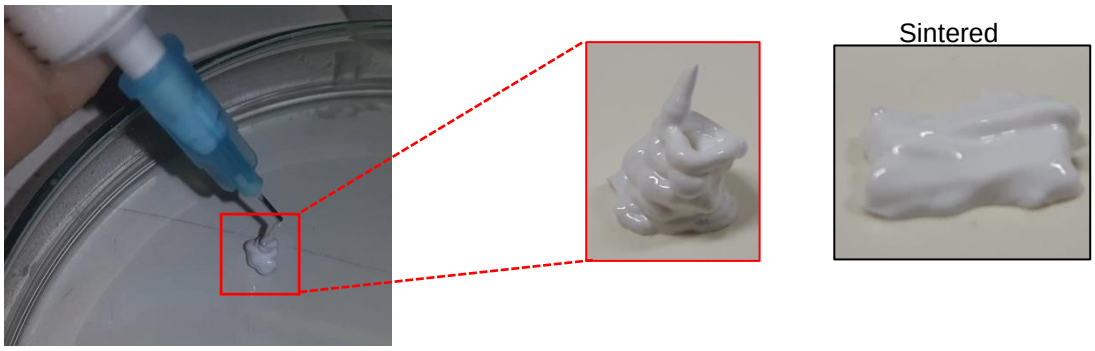

Figure 43. Extrusion of Paste A. A sintered sample is also shown.

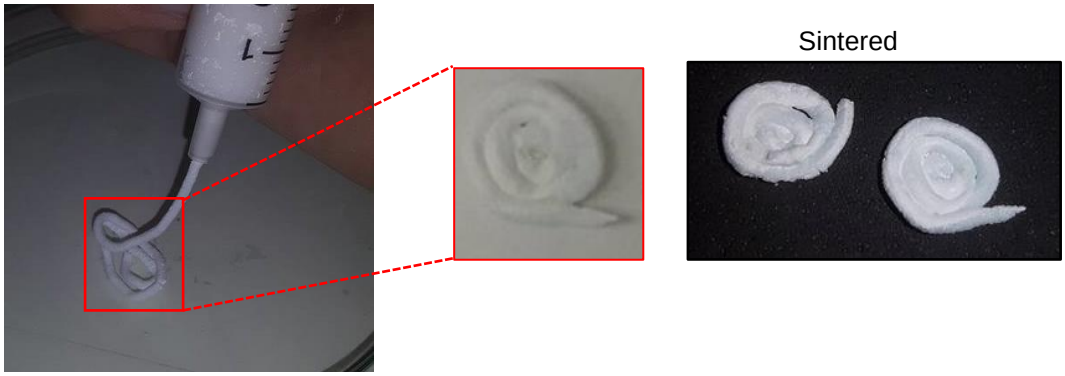

Figure 44. Extrusion of Paste B. Sintered samples are also shown.

The requirements of the pastes are that it must flow with modest pressure through the syringe, retain the desired shape after deposition, dry with minimal shape change after the printing simulation, and sinter to high density. [31] Apparently, both pastes seem to fit these requirements (results on density will be shown and discussed below).

For the extrusion of Paste B, a greater (manual) pressure was required compared to the one used in Paste A, since the consistency of the first one is higher. Despite both pastes were able to be extruded, form fine filaments and support multiple layers, their use in a 3D printer must take into account the specifications of the equipment, since factors such as printing speed, pressure applied on the paste and injector diameter may be critical for the quality of the obtained product.

For comparison purposes, specimens were also produced by molding (Figure 20).

All the specimens were sintered at 1450ºC.

3.4 Caracterization of the specimens

3.4.1 Density measurements

The relative density of the sintered samples (unpolished) produced by manual printing with Paste A and Paste B (considering as reference a typical density value of 6.04 g/cm^3 [54] for yttria zirconia) was determined and is shown in Table 12. For comparison purposes, the density of a commercial sample of yttria zirconia used in labs of dental prosthetics, was also measured.

Table 12. Average relative density of specimens obtained with Paste A (with different content of solids), Paste B and commercial yttria zirconia.

	90	**91**	**92**	**Paste B**	**Sample C**
Relative Density	90.3%	93.2%	96.6%	83.8%	99.3%

For Paste A, all relative density values were above 90%. As expected, the higher the amount the solids, the higher the density. Despite this, these values could still be optimized, for example with better degassing of the paste to prevent pore formation.

In contrast, the density of the specimens produced with Paste B was significantly lower (83.8%). Therefore, it is expected the existence of more space between the particles (*i.e.*, pores).

The relative density of commercial yttria zirconia samples was 99.3%, which is above the value reported by the manufacturer (96 – 99%). [31]

From the results presented above, it may be concluded that samples produced with Paste A higher content of solids are the most promising, since they present a relative density closer to that observed for the commercial material.

3.4.2 Porosity analysis

Porosity was evaluated through an imaging technique for different polished specimens produced with Paste A (90, 91 and 92%), and with paste B. The analysis was also performed for polished commercial Zirconia. Figure 45 shows typical images obtained my optical microscopy for the studied samples. Red areas correspond o the pores identified by ImageJ software.

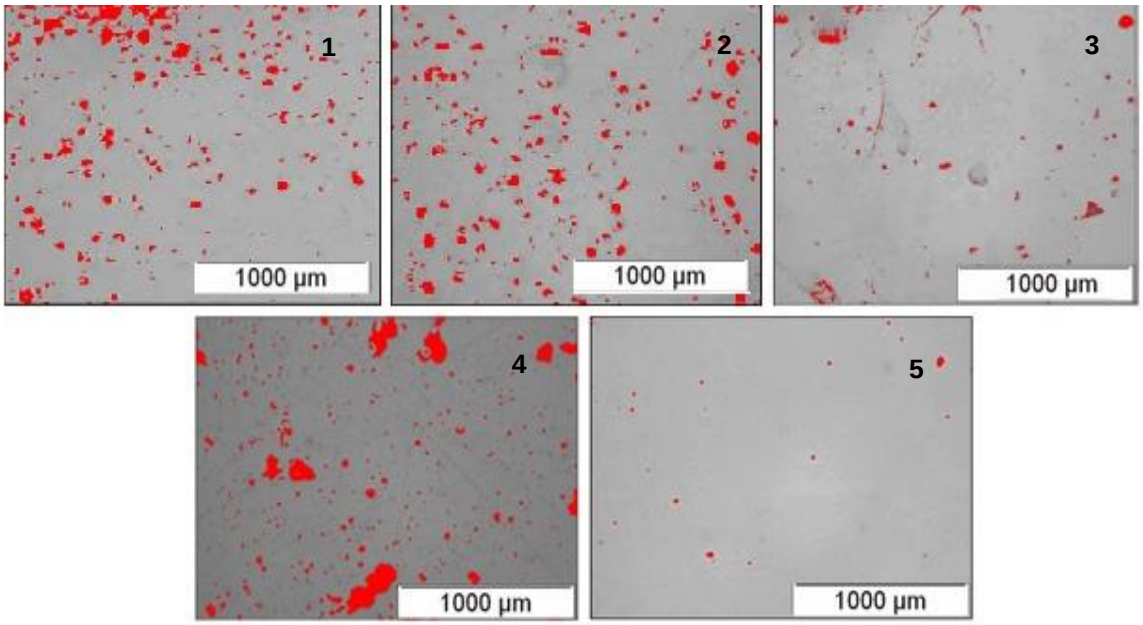

Figure 45. **(1–3)** Paste A: 90%, 91% and 92%, respectively; **(4)** Paste B and **(5)** Commercial Zirconia.

In the three samples produced with paste A (90, 91 and 92%) it was observed the existence of pores randomly distributed. The same is also observed for sample B However, in this case more pores were observed. Existing pores may allow gases or liquids to penetrate the sample, reducing its mechanical strength and eventually the useful life of the material. Pores were almost absent in commercial zirconia (sample C).

Figure 46 presents the percentage of the porous area estimated by the used software. The porosity of the samples of Paste A produced with 90% and 91% of solid content are quite similar, although the values dispersion is relatively high. Samples produced with the higher content of solids (92%) were those that presented the lower percentage of porosity. As expected, from the visual analysis of the images, specimens of paste B were the more porous (porosity 6.06 ± 1.18 %), while samples of commercial zirconia were the less porous (porosity 0.163 ± 0.07%).

In a general way, the porosity results corroborate the tendency found for relative density values: the higher the porosity, the lower the relative density.

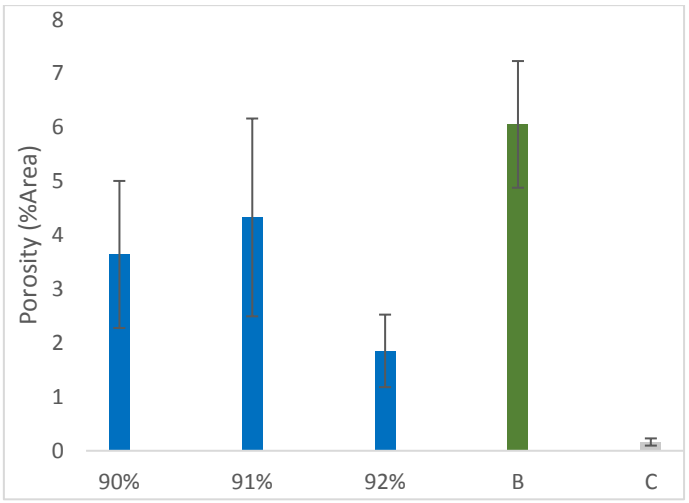

Figure 46. Porosity determined for the specimens produced with Paste A (for 90, 91 and 92% of solids loading), Paste B and commercial zirconia, C.

The distribution of pore size was evaluated for the prepared samples. The pore distribution in sample C is not presented since its porosity is very small.

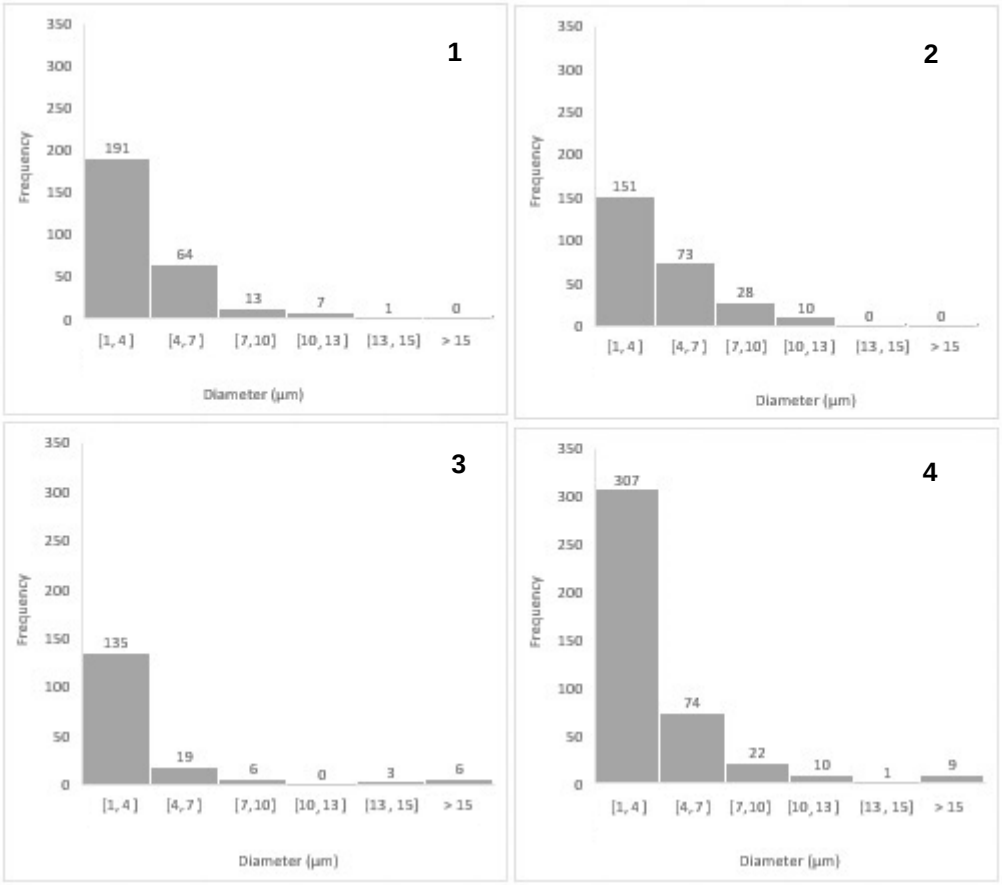

Figure 47. Distribution of sizes of the pores. **(1–3)** Paste A: 90%, 91% and 92%, respectively and **(4)** Paste B.

According to the distribution of sizes of the pores presented in the histograms of Figure 47, it can be observed that all the samples present a high number of pores with small dimensions, being prevalent the pores with diameter lower than 4 µm. As expected from the simple visualization of the optical microscopy images (Figure 45), samples prepared with Paste B are the ones that present the higher number of pores. Among the samples prepared with Paste A, the correspondent to 92% of solids shows a number of pores with dimensions <10 µm significantly lower than the others. More, in comparison with this samples, those prepared with pastes containing 90% and 91% of solids present a higher dispersion of pore sizes.

From the presented results, it was possible to conclude that the 92% is the one that leads to specimens with higher density (close to the reference value) and lower porosity. In this way, Paste A with 92% of solids was chosen as the best one to produce specimens and, consequently, to continue this study.

3.4.4 Surface Morphology/Topography

The surface morphology of samples produced with Paste A with 92% of solids and Paste B was analyzed by SEM. Figure 48 and 49 show typical images obtained for these samples. For comparison purposes, an image of commercial zirconia is also presented (Figure 50).

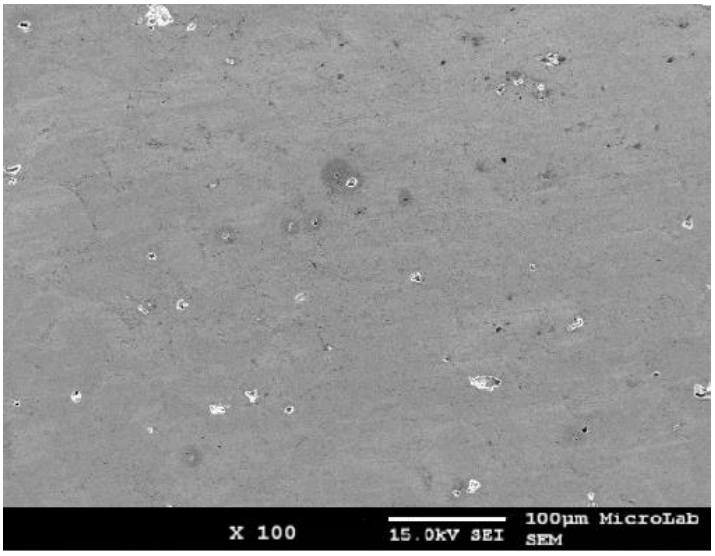

Figure 48. SEM image of sample A.

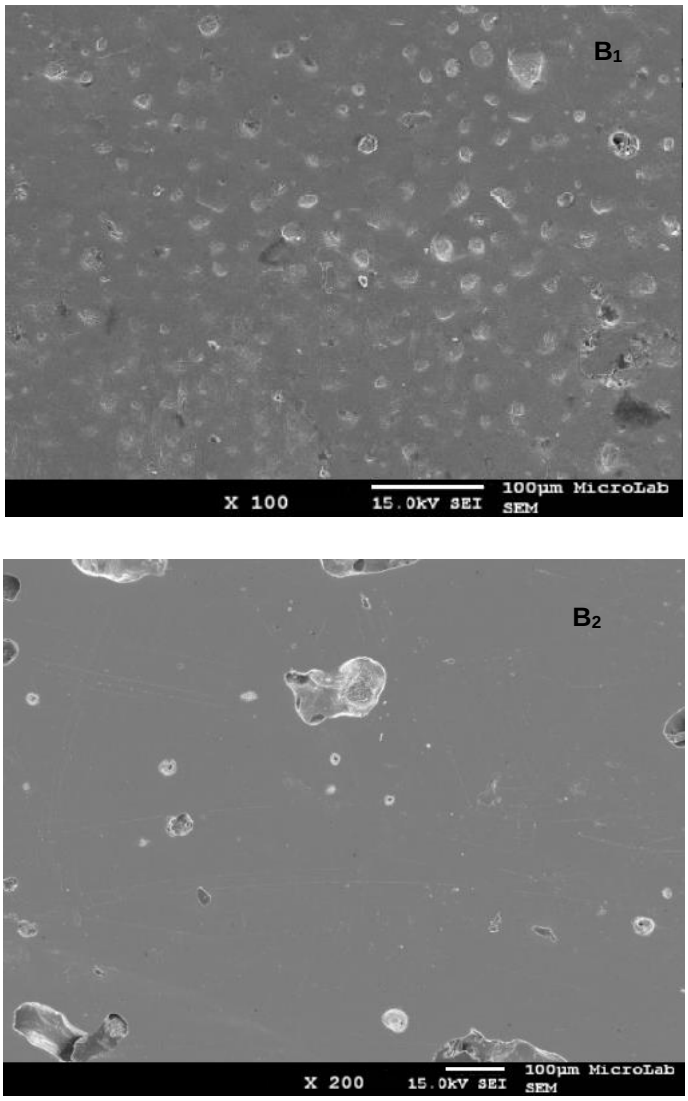

Figure 49. SEM images of sample B.

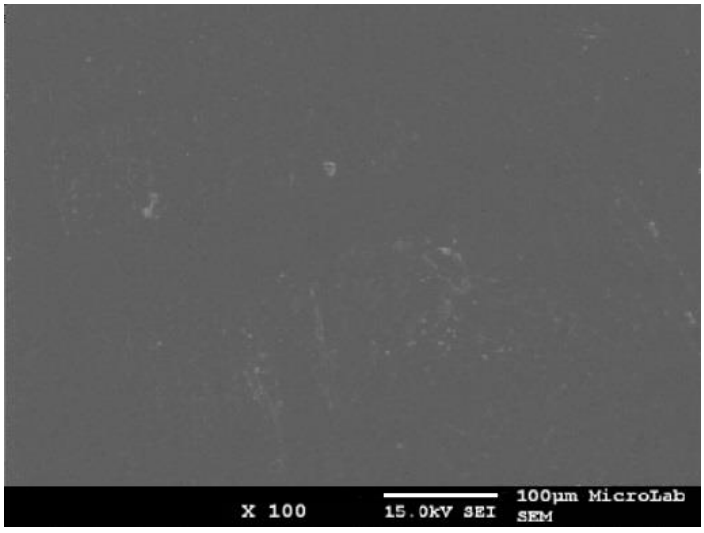

Figure 50. SEM image of commercial zirconia (C).

As observed through the SEM images, sample B is more porous than sample A, in agreement with optical microscopy observation. However, the distribution of pores is not homogeneous: there are places with a high density of pores (Figure 49B$_1$) and others where this is lower (Figure 49B$_2$). Sample C presents a quite uniform surface, similar to that found for Sample A.

The surface topography of the samples between pores was studied by AFM. The following images (Figures 51, 52 and 53) depict the surface of the samples.

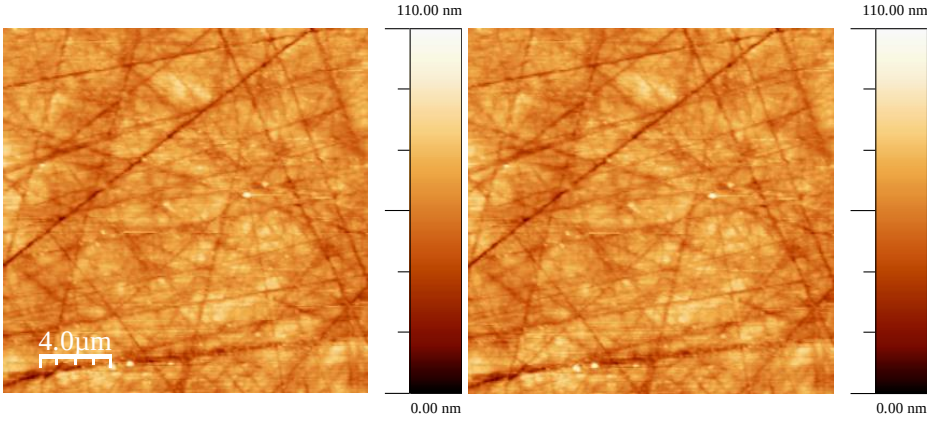

Figure 51. AFM image of the surface area of Sample A, and the respective 3D profile of the surface sample.

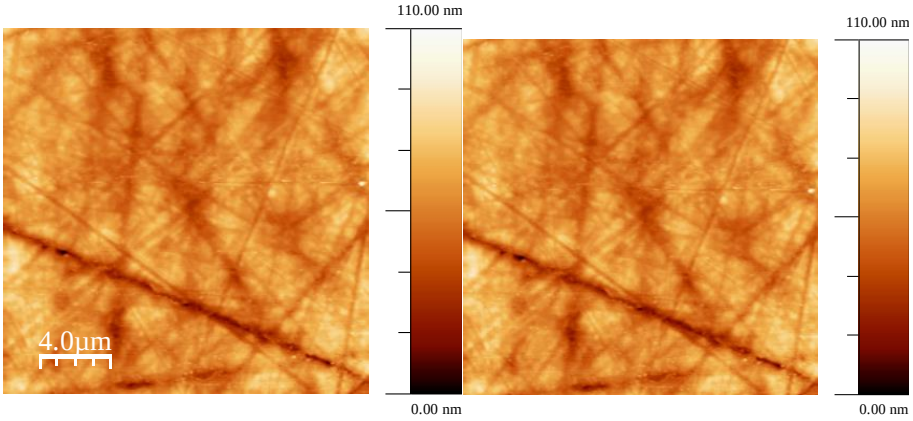

Figure 52. AFM image of the surface area of Sample B, and the respective 3D profile of the surface sample.

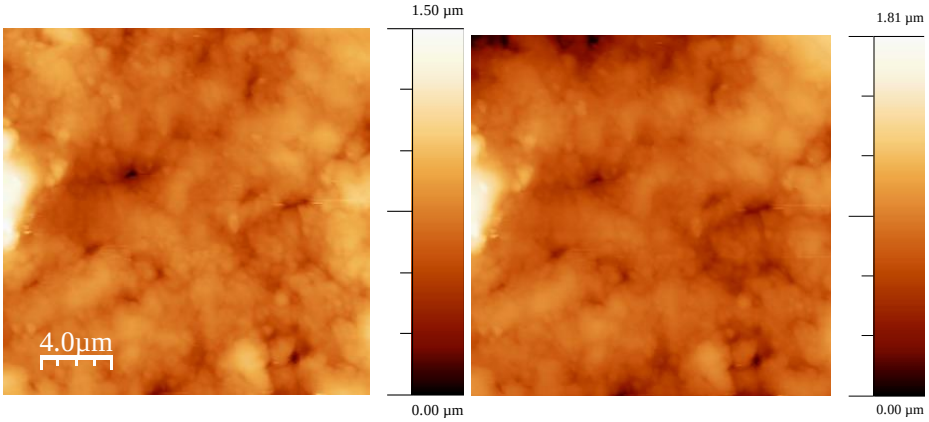

Figure 53. AFM images of the surface area of comercial zirconia sample, and the respective 3D profile of the surface sample.

The topography of the samples A and B are quite similar: some scratches are visible in the surface with a random orientation. In contrast sample C presents a quite different surface: no scratches were observed on the surface, but a granular/globular morphology can be identified. This may be due to the pull out of zirconia grains during the polishing process.

Roughness of intra-oral hard surfaces as zirconia dental restorations have impact on the adhesion and the retention of oral microorganisms. At surface irregularities and asperities (like cracks, porous, and other stagnant sites), bacteria, once attached, can survive longer because they are protected against natural removal forces and also against oral hygiene measures, like toothbrushing. [74] Smooth surfaces (with lower roughness) tend to minimize dental plaque formation, thereby decreasing the occurrence of caries and other dental diseases. [75] Thus, the demand of dental prosthesis with lower surface roughness has been focus of clinical attention.

Figure 54 depicts the average roughness (R_a) determined from a set of AFM images (20µm^2 x 20 µm^2) for the surface of zirconia samples.

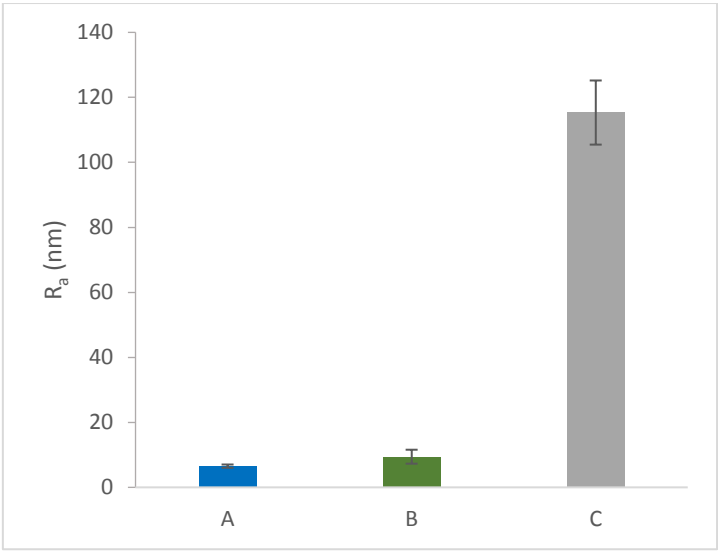

Figure 54. Zirconia mean roughness (R_a).

Samples A and B present values of R_a similar among each other but significantly lower than those found for sample C (about 13 times lower). It must be stressed that these measurements were carried out in inter-pores zone, and thus the porosity does not affect the obtained values. Furthermore, the roughness depends on the material's microstructure which is determined by the grain size. According to the manufacturer the commercial sample (C) presents a grain size of 850 nm. For sample A and B a lower grain size would be expected, since they were prepared with a zirconia powder whose particles had 150 nm and whose sintering temperature was low (1450 ºC), avoiding the grain growth. [76], [77]

3.4.3 Wettability tests

Wettability was studied for all samples, A, B and C, by measuring the contact angle through the sessile drop technique. Figure 55 shows the obtained water contact angles measured for the different specimens.

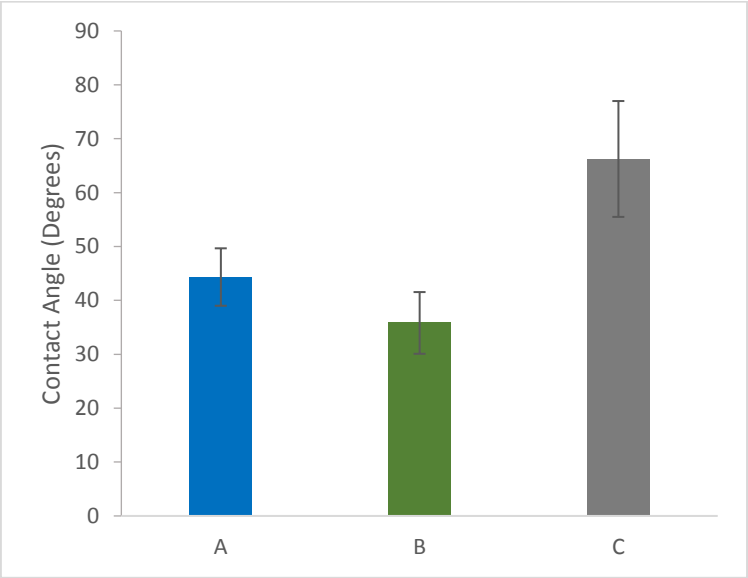

Figure 55. Contact angle for zirconia samples.

Despite the existence of a deviation in the values, all samples had a mean contact angle lower than 90°, which means that a hydrophilic characteristic was maintained in all samples. The same also happens in enamel, which has a contact angle below 60°. [74], [78]

Sample C led to the highest contact angle, 66 ± 10º. Samples A and B present lower and closer values among each other (44 ± 5º and 36 ± 6º, respectively).

Hydrophilicity is an important parameter for dental prosthesis, playing a relevant role in the adhesion of microorganisms and biomacromolecules existent in the oral environment. It also affects the comfort provided by the prosthesis. As referred previously, wettability depends on the chemical and physical characteristics of the surface. In the present case, all surfaces are chemically similar, since the samples

are made of zirconia-based materials. Differences in roughness may explain the different wettability behavior. [79]

Although in previous studies [80] it has been hypothesized, that surface roughness may improve wettability by reducing the contact angle, the wettability behavior in this study was inverse: the surfaces more hydrophilic were the smoothest, A and B.

Wenzel (1936) formulated a model to predict the variation of wettability with roughness. The Wenzel model [81] assumes that the liquid establishes contact with the entire rough surface, filling its depressions (Figure 56A). According to the Wenzel's theory:

$$Cos(\Theta^A) = rcos\Theta \qquad (\mathbf{18})$$

where Θ^A is an apparent contact angle and r is the ratio of the real rough surface area to the projected perfectly smooth surface. Since the parameter r is always greater than 1, this model predicts that the contact angle observed when a liquid wets the surface (Θ<90º) will decrease when the surface becomes more rough (Θ^A <Θ).

In turn, the Cassie-Baxter model (1944) [81] assumes that the liquid does not completely wet the rough surface, due to the air remaining between the depressions of the surface (Figure 56B), being the contact angle measured on a rough surface given by Equation 19:

$$Cos(\Theta^A) = -1 + \phi_{LS}[cos\Theta + 1] \qquad (\mathbf{19})$$

where ϕ_{LS} is the fraction of the liquid-solid interface (hence $\phi_{LS} - 1$ is the fraction of the liquid-air interface).

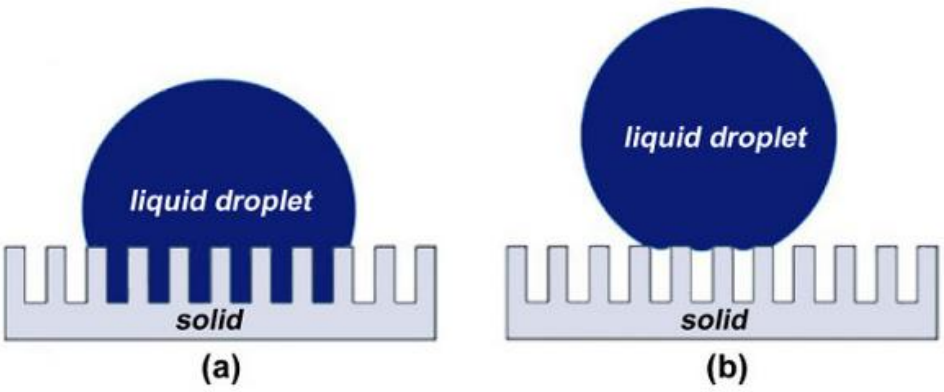

Figure 56. Wenzel (a) and Cassie-Baxter (b) models.

The wettability results obtained in this study seem to be in agreement with the Cassie-Baxter model: the high roughness of samples C shall lead to the formation of air pockets that increase the water contact angle.

It should be stressed that a higher surface roughness its generally associated to a higher tendency to promote bacterial plaque formation. [75] However, several studies referred that bacterial adhesion is favored by the increase of hydrophilicity. [74] In this case, the two factors (roughness and hydrophilicity) act in an opposite way concerning the bacterial adhesion. Studies with microorganisms would have to be performed to clarify this issue. Different bacterial species commonly found in mouth should be used, since it is known that their behavior may differ significantly. [82], [83]

3.4.5 Tribological behavior

Friction and wear are of most importance for the performance of prosthetic materials. Wear tests were performed in to mimetized the local contact of zirconia against zirconia using artificial saliva as lubricant and a load within those found in the mastication process (see section 2.2.4.5). Wear tracks were sought through AFM, but none were found in any of the three samples. This means that the load used does not induce the wear of the tested materials, and that the produced specimens (A and B) offer a wear resistance as good as the commercial sample (C). However, differences were observed concerning the friction coefficient (Figure 57).

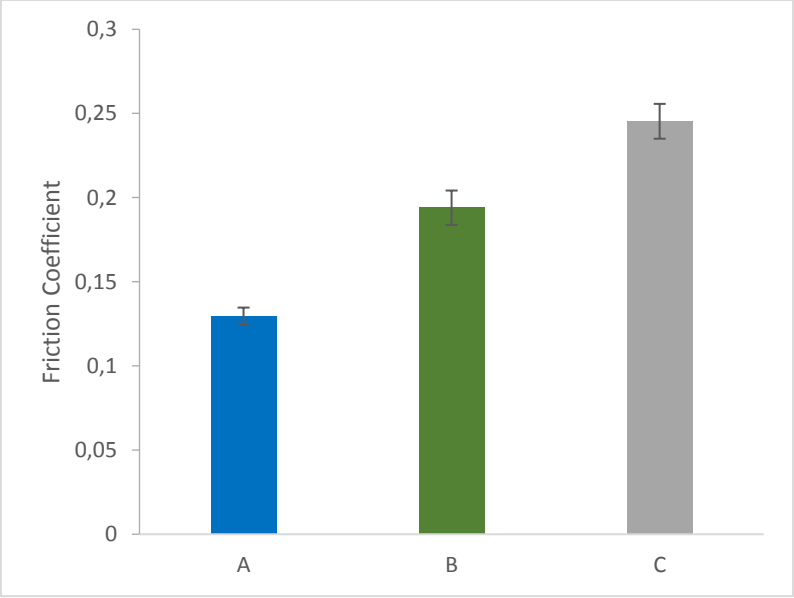

Figure 57. Friction coefficient for zirconia samples.

The friction coefficient depends on the surface energy (adhesion component) and also on the surface roughness (plow component). [67] The obtained results show that the coefficient of friction follows the same trend observed for the roughness, being the highest value achieved for sample C. A higher roughness favors the increase of the friction coefficient. On the other hand, although all surfaces are hydrophilic, a higher contact angle (lower wettability) shall impair the lubrication, increasing the friction coefficient. This means that samples A and B present a better tribological behavior than sample C.

Unlubricated sliding tests already performed on Y_2O_3 doped in zirconia ceramics showed that the friction coefficients varied in the range of 0.5–1. [84], [85] No data was found concerning lubricating systems. The obtained results show that the use of saliva as a lubricant shall contribute to the lower values found for the friction coefficients of the three samples (0.12–0.25), due to the improvement of the lubrication conditions.

3.4.6 Microhardness tests

The Vickers hardness of the studied materials was measured for different loads. The obtained results are presented in Figure 58.

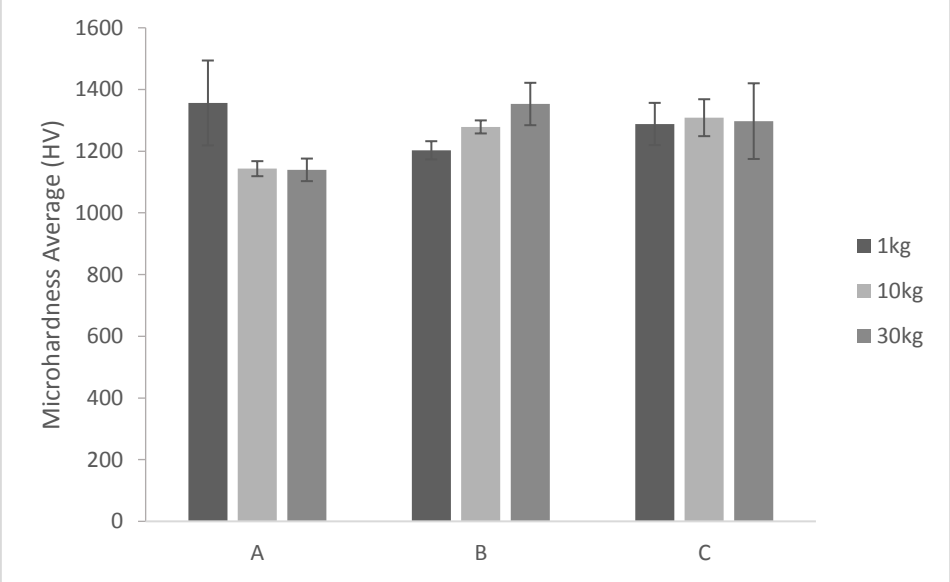

Figure 58. Zirconia microhardness for each sample.

Considering that the reported hardness for yttrium-zirconia is approximately 1250-1300HV [12], [86] it can be seen that the experimental values obtained for the tested samples are close to this reference, independently of the applied load.

No clear effect was observed concerning the applied load: while for samples prepared with Paste A, higher loads lead to lower average hardness values, for samples prepared with Paste B the increase of load results in higher values for hardness and for commercial samples the hardness values are not affected by the load. It must be underlined that observed variations can be due to the heterogeneity, taking into account the error associated to the measurement. The similarity between the obtained values for the three types of samples allow to conclude that despite their different initial compositions, samples A and B present suitable characteristic in terms of hardness.

Understanding the fracture behavior is also essential for the development of "tooth-like" restorative materials. For that, fracture toughness was estimated using a calculation method ($K_{i,c}$) that involved measurements of the lengths of the cracks, which emanate from the corners of Vickers indentation diagonals. The SEM images presented in Figure 59 illustrates this procedure. As referred in section 2.2.4.6, the calculation also requires the knowledge of the material hardness and of its elasticity modulus.

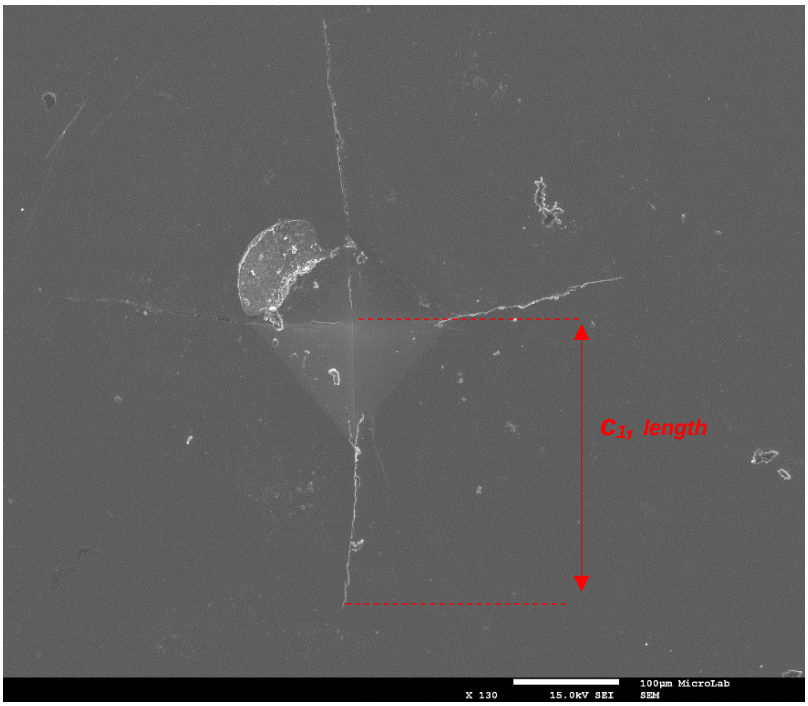

Figure 59. SEM image of an indentation in the commercial sample (C).

Three different equations reported in literature [68] were used to calculate the toughness (Equations 10, 11 and 12, section 2.2.4.6). The microhardness values used were the experimental values for 30 kg (1139.5 HV, 1353 HV and 1297.5 HV for A, B and C, respectively). The obtained results were plotted in Figure 60.

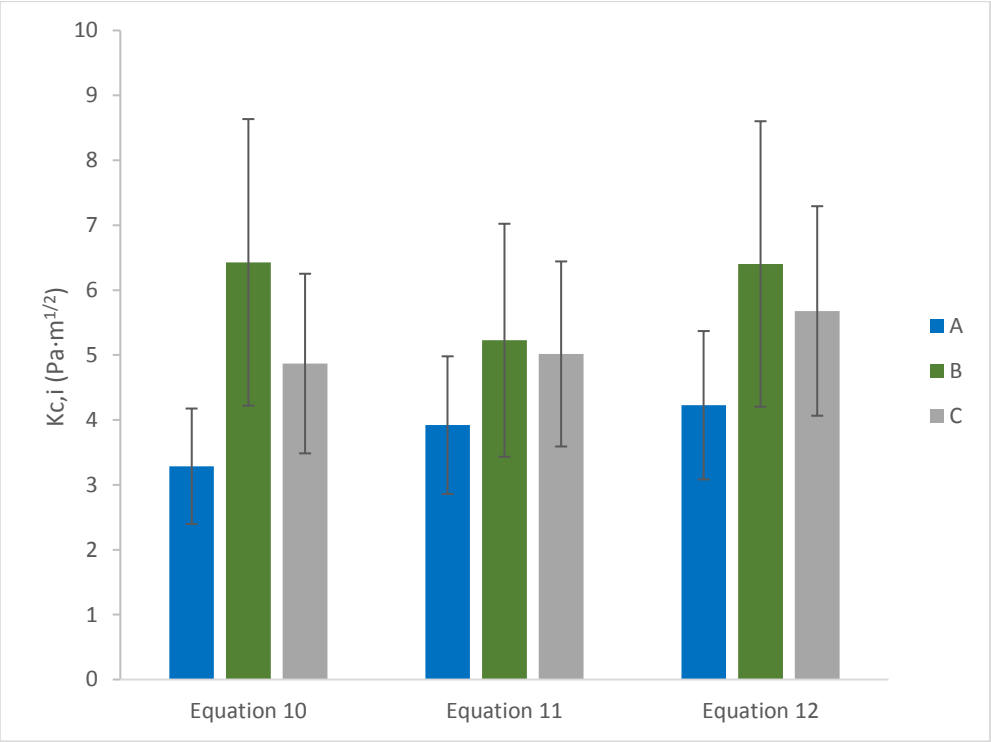

Figure 60. Fracture toughness of samples A, B and C, with the use of different equations.

It was observed that the use of different equations led to different toughness values. However, in qualitative terms the tendency was kept in all cases: the highest value was observed for samples B, followed by C and finally A. The obtained average values, varied in a range of 3–6.5 $Pa \cdot m^{1/2}$, and are lower to those reported for yttria zirconia fracture toughness, 8–10 $Pa \cdot m^{1/2}$ [54]. However, they are within the range observed for dental ceramics used in dental restoration (see Table 2).

Chapter 4 – Conclusions

Zirconia-based pastes containing a dispersant (Dolapix CE64) were formulated and optimized to be used in the production of dental parts by robocasting, based on the study of their rheological behavior. It was concluded that:

1. A concentration of 1% of Dolapix on the solids content allowed to obtain minimum values of consistency and flow rate, in suspensions with 60% solids.
2. Contrarily to what happened with the direct preparation of the pastes with high solids content, the preparation of suspensions based on the evaporation of water (60% to 90% solids loading) resulted in homogeneous pastes.
3. Concentrations > 90% of solids led to the higher values of viscosity.

Taking into account the previous findings, specimens prepared with pastes containing 90%, 91% and 92% of solids and 1% of Dolapix (type A) were characterized and compared with samples obtained from additivated zirconia based-paste provided by CTCV (type B). It was found that:

4. The manual printability of pastes Type A was superior to that of paste B, since the former could pass throw thinner orifices.
5. The increase in the solids content led to an increase of density of the type A materials. B samples presented a lower density than A.
6. From all the tested samples, the one with 92% solids showed the lower porosity, being the pores diameter generally lower than 4 μm.

Comparison with commercial zirconia samples (type C) showed that type A samples with 92% solids are the most promising, concerning density and porosity. Thus, they were selected for further characterization, in comparison with samples of type B and C. The following properties were evaluated: topography/morphology, wettability, tribological behavior, microhardness and toughness. It was observed that:

7. Samples of type A presented the lower roughness (7 ± 1 nm).
8. The water contact angle of samples A and B was significantly lower than that found for samples C, being of the order of 40º.
9. No wear was detected in any of the samples, under loading conditions similar to those observed in the mouth. Samples A led to the lower friction coefficient.
10. The microhardness of all the tested samples falls within the range of values reported for yttria-zirconia commercial samples.
11. The highest values of toughness were obtained for samples B and C. However, all the values are within the typical range found for ceramic dental materials.

Overall, the results showed that specimens produced with Paste A containing 92% solids and 1% Dolapix, presented adequate properties for dental applications. Taking into account the preliminary test of printability, the referred paste may be used for production of dental parts by robocasting.

Chapter 5 – Future work

The work on the optimization of zirconia-based pastes for dental prosthesis through robocasting is still ongoing as part of a project which is running in parallel with the study presented in this thesis. In this way, there are several aspects of research regarding robocasting applied to dental restorations, that must be addressed such as:

1. Optimization of the different printing parameters such as the nozzle diameter, the chosen shear rate and the injection's velocity.
2. Study other properties of the obtained final products (*e.g.*, flexural strength and wear resistance using chewing simulation tests).
3. Study of the microorganisms adhesion behavior onto the produced materials.
4. Study of the protein adsorption onto the produced materials.
5. Evaluation of the cytotoxicity of the produced materials.

References

[1] Z. R. Zhou and J. Zheng, “Tribology of dental materials: a review,” *J. Phys. D. Appl. Phys.*, vol. 41, no. 11, p. 113001, 2008.

[2] E. Atzeni and A. Salmi, “Evaluation of additive manufacturing (AM) techniques for the production of metal-ceramic dental restorations,” *J. Manuf. Process.*, vol. 20, pp. 40–45, 2015.

[3] S. Roy and B. Basu, “Mechanical and tribological characterization of human tooth,” *Mater. Charact.*, vol. 59, no. 6, pp. 747–756, 2008.

[4] P. Gupta and M. R. Sankar, “Advanced Materials State of Art on Tribomechanical andTribo chemical Wear of Human Dental Enamel,” vol. 3, no. 1, pp. 119–126, 2013.

[5] M. A. Garrido, I. Giráldez, L. Ceballos, M. T. G. del Río, and J. Rodríguez, “Nanotribological behaviour of tooth enamel rod affected by bleaching treatment,” *Wear*, vol. 271, no. 9–10, pp. 2334–2339, 2011.

[6] A. A. Madfa and X. G. Yue, “Dental prostheses mimic the natural enamel behavior under functional loading: A review article,” *Jpn. Dent. Sci. Rev.*, vol. 52, no. 1, pp. 2–13, 2016.

[7] A. Branco, A. P. Valagão, and C. Figueiredo-Pina, “Study of the effect of pH and of the presence of remineralizing agents on teeth whitening treatments with doped mixtures based on hydrogen peroxide,” pp. 1–31.

[8] G. Balooch, G. W. Marshall, S. J. Marshall, O. L. Warren, S. A. S. Asif, and M. Balooch, “Evaluation of a new modulus mapping technique to investigate microstructural features of human teeth,” *J. Biomech.*, vol. 37, no. 8, pp. 1223–1232, 2004.

[9] V. Imbeni, J. J. Kruzic, G. W. Marshall, S. J. Marshall, and R. O. Ritchie, “The dentin–enamel junction and the fracture of human teeth,” *Nat. Mater.*, vol. 4, no. 3, pp. 229–232, 2005.

[10] H. H. K. H. Xu *et al.*, “Indentation Damage and Mechanical Properties of Human Enamel and Dentin,” *J. Dent. Res.*, vol. 77, no. 3, pp. 472–480, 1998.

[11] T. K. James Zhijian Shen, “Advanced Ceramics for Dentistry,” 2014. [Online]. Available: https://books.google.pt/books?id=Y-9jwrHs0WEC&pg=PR13&lpg=PR13&dq=Advanced+Ceramics+for+Dentistry&source=bl&ots=-QTGTJkfne&sig=0qrwzxOOGB1DnFZkwGQ75x8fYFg&hl=pt-PT&sa=X&ved=0ahUKEwi6jfTjqKLXAhVEchQKHcTCDqgQ6AEIYjAI#v=onepage&q=Advanced Ceramics for Dentis. [Accessed: 07-Nov-2017].

[12] F. A. T. Rodrigues, “Efeito do branqueamento dentário com peróxido de hidrogénio na morfologia , hidrofilicidade , propriedades mecânicas e tribológicas do esmalte,” pp. 1–54, 2015.

[13] S. D. Heintze, G. Zappini, and V. Rousson, “Wear of ten dental restorative materials in five wear simulators--results of a round robin test.,” *Dent. Mater.*, vol. 21, no. 4, pp. 304–17, 2005.

[14] R. Lewis and R. S. Dwyer-Joyce, “Wear of human teeth: a tribological perspective,” *Proc. I MECH E Part J J. Eng. Tribol.*, vol. 219, no. 1, pp. 2–19, 2005.

[15] K. Mundhe, V. Jain, G. Pruthi, and N. Shah, “Clinical study to evaluate the wear of natural enamel antagonist to zirconia and metal ceramic crowns,” *J. Prosthet. Dent.*, vol. 114, no. 3, pp. 358–363, 2015.

[16] L. H. Mair, T. A. Stolarski, R. W. Vowles, and C. H. Lloyd, “Wear: mechanisms, manifestations and measurement. Report of a workshop,” *J. Dent.*, vol. 24, no. 1–2, pp. 141–148, 1996.

[17] E. Sajewicz, “Effect of saliva viscosity on tribological behaviour of tooth enamel,” *Tribol. Int.*, vol. 42, no. 2, pp. 327–332, 2009.

[18] R. A. Gittens *et al.*, “A review on the wettability of dental implant surfaces II: Biological and clinical aspects,” *Acta Biomater.*, vol. 10, no. 7, pp. 2907–2918, 2014.

[19] L. Y. Chen, Q. Q. Fang, W. Z. Jiang, X. P. Liao, J. Y. Ye, and H. Le Jin, “Study of the Hydrophobic Properties of the Surface of an Enamel Material,” *Mater. Sci. Forum*, vol. 789, pp. 178–182, 2014.

[20] H. J. Busscher, “Modern Approaches to Wettability: Theory and Applications.” [Online]. Available: https://books.google.pt/books?id=FhsGCAAAQBAJ&pg=PA249&lpg=PA249&dq=Wettability+of+Surfaces+in+the+Oral+Cavity&source=bl&ots=rcrC7ao6xI&sig=XgcPY_3ySYoM6CWYjhlrIF_7MnA&hl=pt-PT&sa=X&ved=0ahUKEwjdnrmdzazXAhVDvhQKHSozDnsQ6AEIQTAD#v=onepage&q=Wettability of. [Accessed: 07-Nov-2017].

[21] K. J. Kubiak, M. C. T. Wilson, T. G. Mathia, and P. Carval, “Wettability versus roughness of engineering surfaces,” in *Wear*, 2011, pp. 523–528.

[22] J. Pihlaja, “Treatment Outcome of Zirconia Single Crowns and Fixed Dental Prostheses,” University of Oulu Graduate School, Doctoral dissertation, 2016.

[23] E. Homaei, K. Farhangdoost, E. H. N. Pow, J. P. Matinlinna, M. Akbari, and J. K. H. Tsoi, “Fatigue resistance of monolithic CAD/CAM ceramic crowns on human premolars,” *Ceram. Int.*, vol. 42, no. 14, pp. 15709–15717, 2016.

[24] “Dental Crowns.” [Online]. Available: http://fgdentalcare.com/dentalcrowns_bridges_venears.php. [Accessed: 23-Apr-2017].

[25] Usha, G, T. . Prashanth, R. N. Roopa, G. Yashwanth, and Murtuza, “Advanced Ceramics a Review of Material Science,” *Journal of Dental Sciences and Research*, vol. 5, no. 2. pp. 5–11,

2014.

[26] Invibio Biomaterials Solutions and C. a D. Cam, “New Material Options for Innovation in Restorative and Prosthetic Dentistry,” pp. 1–8, 2011.

[27] J. Chevalier, *What future for zirconia as a biomaterial?*, vol. 27, no. 4. Elsevier Ltd., 2006.

[28] I. Denry and J. R. Kelly, “State of the art of zirconia for dental applications,” *Dent. Mater.*, vol. 24, no. 3, pp. 299–307, 2008.

[29] P. Pittayachawan, “Comparative study of physical properties of zirconia based dental ceramics,” *Dr. thesis, UCL (University Coll. London).*, 2009.

[30] E. E. Daou, “The zirconia ceramic: strengths and weaknesses.,” *Open Dent. J.*, vol. 8, pp. 33–42, 2014.

[31] “ZirCad e.max.” [Online]. Available: http://www.ivoclarvivadent.com/en/p/all/products/all-ceramics/ips-emax-technicians/ips-emax-zircad. [Accessed: 11-Nov-2017].

[32] R. Van Noort, “The future of dental devices is digital,” *Dent. Mater.*, vol. 28, no. 1, pp. 3–12, 2012.

[33] V. T. Le, H. Paris, and G. Mandil, “Process planning for combined additive and subtractive manufacturing technologies in a remanufacturing context,” *J. Manuf. Syst.*, vol. 44, pp. 243–254, 2017.

[34] E. J. Bae, I. Do Jeong, W. C. Kim, and J. H. Kim, “A comparative study of additive and subtractive manufacturing for dental restorations,” *J. Prosthet. Dent.*, vol. 118, no. 2, pp. 187–193, 2017.

[35] N. Guo and M. C. Leu, “Additive manufacturing: Technology, applications and research needs,” *Front. Mech. Eng.*, vol. 8, no. 3, pp. 215–243, 2013.

[36] D. Drummer, C. Williams, and J. Parthasarathy, “Additive Manufacturing: Innovations, Advances, and Applications,” no. 15, pp. 389–401, 2013.

[37] A. Ambrosi and M. Pumera, “3D-printing technologies for electrochemical applications,” *Chem. Soc. Rev.*, vol. 45, no. 10, pp. 2740–2755, 2016.

[38] D. S. Reis, “Aplicação de alumina em robocasting,” 2017.

[39] M. Leary *et al.*, “Additive manufacture of custom radiation dosimetry phantoms: An automated method compatible with commercial polymer 3D printers,” *Mater. Des.*, vol. 86, pp. 487–499, 2015.

[40] H. N. Mai, K. B. Lee, and D. H. Lee, “Fit of interim crowns fabricated using photopolymer-jetting 3D printing,” *J. Prosthet. Dent.*, vol. 118, no. 2, pp. 208–215, 2017.

[41] M. Faes, H. Valkenaers, F. Vogeler, J. Vleugels, and E. Ferraris, “Extrusion-based 3D printing

of ceramic components," *Procedia CIRP*, vol. 28, pp. 76–81, 2015.

[42] J. A. Lewis, J. E. Smay, J. Stuecker, and J. Cesarano, "Direct ink writing of three-dimensional ceramic structures," *J. Am. Ceram. Soc.*, vol. 89, no. 12, pp. 3599–3609, 2006.

[43] E. Feilden, E. G. T. Blanca, F. Giuliani, E. Saiz, and L. Vandeperre, "Robocasting of structural ceramic parts with hydrogel inks," *J. Eur. Ceram. Soc.*, vol. 36, no. 10, pp. 2525–2533, 2016.

[44] J. Cesarano, "A Review of Robocasting Technology," *MRS Proc.*, vol. 542, pp. 133–139, 2011.

[45] N. R. F. A. Silva, L. Witek, P. G. Coelho, V. P. Thompson, E. D. Rekow, and J. Smay, "Additive CAD/CAM process for dental prostheses," *J. Prosthodont.*, vol. 20, no. 2, pp. 93–96, 2011.

[46] T. Ii, "Reologia e Estrutura dos Alimentos Viscosidade de Fluidos Newtonianos e."

[47] E. Peng *et al.*, "Robocasting of dense yttria-stabilized zirconia structures," *J. Mater. Sci.*, vol. 53, no. 1, pp. 1–27, 2017.

[48] S. P. Rao, S. S. Tripathy, and A. M. Raichur, "Dispersion studies of sub-micron zirconia using Dolapix CE 64," *Colloids Surfaces A Physicochem. Eng. Asp.*, vol. 302, no. 1–3, pp. 553–558, 2007.

[49] E. Özkol, J. Ebert, K. Uibel, A. M. Wätjen, and R. Telle, "Development of high solid content aqueous 3Y-TZP suspensions for direct inkjet printing using a thermal inkjet printer," *J. Eur. Ceram. Soc.*, vol. 29, no. 3, pp. 403–409, 2009.

[50] M. Biswas and A. M. Raichur, "Dispersion of zirconia in the presence of dolapix PC75," *J. Dispers. Sci. Technol.*, vol. 31, no. 9, pp. 1173–1177, 2010.

[51] J. G. da Silva, "REOLOGIA E MICROESTRUTURA NA ESTABILIZAÇÃO DE SUSPENSÕES CONCENTRADAS DE Al2O3," p. 134, 2003.

[52] P. Kohorst, M. P. Dittmer, L. Borchers, and M. Stiesch-Scholz, "Influence of cyclic fatigue in water on the load-bearing capacity of dental bridges made of zirconia," *Acta Biomater.*, vol. 4, no. 5, pp. 1440–1447, 2008.

[53] S. Zürcher and T. Graule, "Influence of dispersant structure on the rheological properties of highly-concentrated zirconia dispersions," *J. Eur. Ceram. Soc.*, vol. 25, no. 6, pp. 863–873, 2005.

[54] "Yttria Zirconia." [Online]. Available: http://www.zircomet.com/det/10951/Yttria-Stabilised-Zirconium-Oxides/,. [Accessed: 26-Jul-2017].

[55] "Powdered Sugar as a Binder." [Online]. Available: https://www.google.com/patents/EP1430158A4?cl=en. [Accessed: 11-Nov-2017].

[56] "Modular Advanced Rheometer System," *Fisher Thermo Scientific*. [Online]. Available: http://www.thermo.com.cn/Resources/200802/productPDF_105.pdf. [Accessed: 03-Nov-2017].

[57] I. Mazali, “Determinação da densidade de sólidos pelo método de Arquimedes,” *http://lqes.iqm.unicamp.br/*, 2010. [Online]. Available: http://scholar.google.com/scholar?hl=en&btnG=Search&q=intitle:Determina??o+da+Densidade+de+S?lidos+pelo+M?todo+de+Arquimedes#0. [Accessed: 10-Sep-2017].

[58] F. T. Rodrigues, A. P. Serro, M. Polido, A. Ramalho, and C. G. Figueiredo-Pina, “Effect of bleaching teeth with hydrogen peroxide on the morphology, hydrophilicity, and mechanical and tribological properties of the enamel,” *Wear*, vol. 374–375, pp. 21–28, 2017.

[59] A. Force and M. Afm, “Basic Theory,” *Energy*, vol. 67, no. 1, pp. 1–8, 1948.

[60] B. Hafner and B. Hafner, “Scanning Electron Microscopy Primer,” *Cities*, pp. 1–29, 2007.

[61] “Scanning Electron Microscope.” [Online]. Available: http://www.mee-inc.com/hamm/scanning-electron-microscopy-sem/. [Accessed: 21-Oct-2017].

[62] C. G. Figueiredo-Pina *et al.*, “Tribological behaviour of unveneered and veneered lithium disilicate dental material,” *J. Mech. Behav. Biomed. Mater.*, vol. 53, pp. 226–238, 2016.

[63] W. Abdallah *et al.*, “Fundamentals of Wettability,” *Oilf. Rev.*, pp. 44–61, 2007.

[64] N. Lawson, “Composite Dental Materials: Wear,” *Ref. Modul. Mater. Sci. Mater. Eng.*, no. October 2015, p. , 2016.

[65] D. Cristina, “PhD program in Advanced Materials and Processing Course Seminário 2016 – 3ªEdição Seminar À Procura do Atrito Zero,” 2016.

[66] “Masticatory Force.” [Online]. Available: https://en.wikipedia.org/wiki/Masticatory_force. [Accessed: 23-Oct-2017].

[67] C. G. Figueiredo-Pina *et al.*, “Effect of feldspar porcelain coating upon the wear behavior of zirconia dental crowns,” *Wear*, vol. 297, no. 1–2, pp. 872–877, 2013.

[68] F. Sergejev and M. Antonov, “Comparative study on indentation fracture toughness measurements of cemented carbides,” *Proc. Est. Acad. Sci. Eng*, vol. 12, no. 4, pp. 388–398, 2006.

[69] P. a Dearnley, “A review of metallic, ceramic and surface-treated metals used for bearing surfaces in human joint replacements.,” *Proc. Inst. Mech. Eng. H.*, vol. 213, no. 2, pp. 107–135, 1999.

[70] F. Rickhey, K. P. Marimuthu, J. H. Lee, H. Lee, and J. H. Hahn, “Evaluation of the fracture toughness of brittle hardening materials by Vickers indentation,” *Eng. Fract. Mech.*, vol. 148, pp. 134–144, 2015.

[71] Zschimmer&Schwarz, “Mechanisms of action of deflocculants and dispersants in ceramic

bodies," *Zschimmer Schwarz GmbH Co KG*, pp. 1–15, 2013.

[72] D. Y. Zirconia, "Electronic Supporting Information (ESI)," pp. 1–21.

[73] T. A. Baer, J. Cesarano III, P. Calvert, J. Cesarano, T. A. Baer, and P. Calvert, "Recent developments in freeform fabrication of dense ceramics from slurry deposition," *Solid Free. Fabr. Proceedings, Sept. 1997*, pp. 25–32, 1997.

[74] M. Quirynen and C. M. L. Bollen, "The influence of surface roughness and surface-free energy on supra- and subgingival plaque formation in man: A review of the literature," *Journal of Clinical Periodontology*, vol. 22, no. 1. pp. 1–14, 1995.

[75] M. D. McConnell, Y. Liu, A. P. Nowak, S. Pilch, J. G. Masters, and R. J. Composto, "Bacterial plaque retention on oral hard materials: Effect of surface roughness, surface composition, and physisorbed polycarboxylate," *J. Biomed. Mater. Res. - Part A*, vol. 92, no. 4, pp. 1518–1527, 2010.

[76] B. STAWARCZYK, A. EMSLANDER, M. ROOS, B. SENER, F. NOACK, and C. KEUL, "Zirconia ceramics, their contrast ratio and grain size depending on sintering parameters," *Dent. Mater. J.*, vol. 33, no. 5, pp. 591–598, 2014.

[77] B.-N. KIM, T. S. SUZUKI, K. MORITA, H. YOSHIDA, J.-G. LI, and H. MATSUBARA, "Evaluation of densification and grain-growth behavior during isothermal sintering of zirconia," *J. Ceram. Soc. Japan*, vol. 125, no. 4, pp. 357–363, 2017.

[78] R. M. A. E. G. H. Glantz, P.O. Baier, R.E. Attstrom, "Comparative clinical wettability of teeth and intraoral mucosa," *J. Adhes. Sci. Technol.*, vol. 5, no. 5, pp. 401–408, 1991.

[79] A. Noro, M. Kaneko, I. Murata, and M. Yoshinari, "Influence of surface topography and surface physicochemistry on wettability of zirconia (tetragonal zirconia polycrystal)," *J. Biomed. Mater. Res. - Part B Appl. Biomater.*, vol. 101 B, no. 2, pp. 355–363, 2013.

[80] W. M. Al-Omari, C. a Mitchell, and J. L. Cunningham, "Surface roughness and wettability of enamel and dentine surfaces prepared with different dental burs.," *J. Oral Rehabil.*, vol. 28, pp. 645–650, 2001.

[81] G. Bracco and B. Holst, *Surface science techniques*, vol. 51, no. 1. 2013.

[82] H. K. Kuramitsu, X. He, R. Lux, M. H. Anderson, and W. Shi, "Interspecies Interactions within Oral Microbial Communities," *Microbiol. Mol. Biol. Rev.*, vol. 71, no. 4, pp. 653–670, 2007.

[83] "Bacterial Mouth Infections." [Online]. Available: https://emedicine.medscape.com/article/1081424-overview. [Accessed: 20-Nov-2017].

[84] M. Woydt, J. Kadoori, K. H. Habig, and H. Hausner, "Unlubricated sliding behaviour of various zirconia-based ceramics," *J. Eur. Ceram. Soc.*, vol. 7, no. 3, pp. 135–145, 1991.

[85] H. R. Pasaribu, J. W. Sloetjes, and D. J. Schipper, “Friction reduction by adding copper oxide into alumina and zirconia ceramics,” *Wear*, vol. 255, no. 1–6, pp. 699–707, 2003.

[86] F. J. L. Alves, “Materiais de construção mecânica ii (em307),” vol. 1704, no. 1742, pp. 1–12, 2005.